INTERNATIONAL ATOMIC ENERGY AGENCY
UNITED NATIONS EDUCATIONAL, SCIENTIFIC AND CULTURAL ORGANIZATION

INTERNATIONAL CENTRE FOR THEORETICAL PHYSICS
34100 TRIESTE (ITALY) - P.O.B. 586 - MIRAMARE - STRADA COSTIERA 11 - TELEPHONES: 224281/2/3/4/5/6
CABLE: CENTRATOM - TELEX 460392-1

SMR/113 - 11

AUTUMN COLLEGE

ON

THE TROPOSPHERE, STRATOSPHERE AND MESOSPHERE

10 September - 19 October 1984

SUBSURFACE PROPAGATION

Chapter 1 - Introduction

Chapter 2 - Electromagnetic theory of subsurface propagation

P. DELOGNE

Laboratoire de Télécommunications
et d'Hyperfréquences
Université Catholique de Louvain
Louvain-La-Neuve
Belgium

CONTENTS

CHAPTER 1 INTRODUCTION

1.1. OBJECTIVES

Radio waves do not propagate very well in tunnels. This fact is experienced every day by many car drivers, but what is here merely a discomfort becomes a serious drawback for people working below the earth surface. This is particularly true in the mines, wherein mobile radio communications are presently considered as a need for increased safety and productivity. Very surprisingly, the subject of electromagnetic wave propagation in subsurface works was nearly unexplored before the end of the decade 1960-1970. Since then, substantial research efforts have been made on this topic in several countries and a good knowledge of the involved propagation mechanisms is now available.

It is the aim of this course to provide an introduction to the subject of subsurface radio wave propagation and to the related topic of leaky feeders. The material of this course has been taken from the author's book "Leaky feeders and subsurface radio communication" published by Peter Peregrinus in 1982 and which is proposed for further study, being the only existing book on the subject. The mathematical appendixes have been taken as such from the book. The bibliography given at the end of the present notes is also wider than strictly required since it contains many interesting articles that are not explicitely referenced in the text. Of course, sentences of the type "it can be shown" generally refer to proofs given in the book.

1.2. MATERIAL PROPERTIES

The question of the electrical parameters of natural rock materials is rather complex and it could be the subject of a whole book. The fine structure of many natural rocks is crystalline. The crystals are always very small compared to the wavelengths used in subsurface radiocommunications and, insofar as they have no preferential orientation, we may consider that the bulk electrical properties of the material are isotropic. In fact they frequently do have a preferred orientation due to the geological stratification and this creates some anisotropy. This effect will be neglected here because it is completely negligible compared to the wide spread and high variability of the values of electrical parameters. These are the dielectric constant κ, the permeability σ, and the conductivity σ.

Excluding rocks with a high concentration in metals of the ferromagnetic group, including iron, nickel and cobalt, the permeability of natural materials is very close to that of vacuum $\mu_o = 4\pi\ 10^{-7}$ H/m. Unless otherwise mentioned, this value will be adopted throughout.

The dielectric constant and the conductivity of rocks, on the contrary, are highly variable. Dielectric constants range from 2 to 70 but more frequently from 4 to 10. Conductivities range from 10^{-6} to 1 mho/m and may be spread on more than two decades for a given type of material at a fixed frequency. In general both κ and σ increase with the water content. As a general rule the conductivity increases and the dielectric constant decreases with frequency, because of dispersion effects; these evolutions are not independant for they are related by Kramers and Kronig's relations (Landau and Lifshitz, 1960), which may be used to check the validity of experimental data. Furthermore the conductivity and the dielectric constant may depend on the pressure (Onsager effect). Extremely high pressures exist at large depths, but when a tunnel is bored, decompression occurs in the surrounding rock. As a result the pressure effect may be neglected.

Conductivity and dielectric constant of samples can be measured with a good accuracy in the laboratory. One should be very careful on the validity of such measurements because of the difficulty of taking a sample and bringing it to the laboratory without modifying the electrical parameters. Furthermore, values obtained this way are only relative to a small sample and are not necessarily representative if the ground is inhomogeneous. In situ measurements and particularly the careful comparison of propagation data with calculations made on adequate models are undoubtedly preferable. They are also more difficult to obtain.

Figure 1.1 shows the range of values obtained by J.C. Cook (1975) from laboratory measurements on various rock materials and on several types of concrete at four frequencies. We have only shown the global range covered by the measurements on each type of rock : the reader interested in detailed values is referred to the original paper. The distinction between wet and dry material has been made only for those materials where this yields larger differences than the spread between samples of the same type of rock.

Although the values shown on this figure result from an intensive series of measurements, they should still be considered as indicative. Values lying outside

the indicated range may be encountered in practice. We are here particularly interested in the electrical properties of coal and of the surrounding rock. As the figure shows, the conductivity of coal is rather low. A remarkable property used in one projected radio communication system is that the conductivity of the roof in coal mines is much larger than that of the seam. Emslie and Lagace (1978) have reported conductivities of 3 10^{-5} to 4 10^{-3} for coal and 7.7 10^{-3} to 1.09 mho/m for the roof in U.S. mines at medium frequencies. In the various cases the ratio of the conductivities was between 75 and 5400. Values measured by Balanis et al. (1978) for bituminous coal up to 100 MHz are consistent with this, except that the dielectric constant of coal is higher at low frequencies : 16 to 41 at 500 kHz and 10 to 34 at 1 MHz. These authors have observed that the conductivity and the dielectric constant may vary by a factor of about 4 with the direction, but that these parameters are nearly intensitive to temperature up to 370°C. They also report measurements made at 9 GHz for bituminous coal : κ = 3.4 to 3.9 and σ = 0.12 to 0.73 mho/m.

A characteristic frequency for a given medium is the transition frequency f_t defined by the equality $2\pi f_t \varepsilon = \sigma$. Below this frequency, conduction currents in the material are more important than displacement currents and the material may be regarded as a conductor. Above this frequency, the inverse situation occurs and the material behaves rather as a dielectric. The last column of Fig. 1.1 gives, for each of the four frequencies considered, a mean value of the ratio f/f_t, where f_t has been calculated using the mean values of σ and κ at the frequency f.

For a quick reference, Figure 1.2 shows the real and imaginary parts of the propagation constant for a uniform plane wave in a homogeneous medium

$$\Gamma = \alpha + j\beta = (j\omega\varepsilon_o \kappa + \sigma)\, j\omega\mu_o \qquad (1.1)$$

for κ = 10 and for various conductivities. Scales are also drawn for the penetration (or skin) depth

$$\delta = 1/\alpha \qquad (1.2)$$

and for the wavelength

$$\lambda = 2\pi/\beta \qquad (1.3)$$

At the transition frequency, which is marked by a dot on the curves, the argument of Γ is equal to $3\pi/8$. It should however not be overlooked that the material properties, including the transition frequency, vary with frequency. This figure may also be used to obtain the complex refractive index n, which is defined by

$$n = \Gamma/(jk_o) \qquad (1.4)$$

where $k_o = \omega\sqrt{\varepsilon_o\mu_o}$ is also shown on the figure. It is obvious from the figure that through-the-ground propagation suffers very high attenuations excepted at low frequencies or in very low conductivity media like salt and some coal types.

1.3. NATURAL PROPAGATION IN EMPTY TUNNELS

We start our analysis of subsurface propagation by considering a straight tunnel and we assume that it does not contain any object and particularly any axial conductor. This is a very rare situation, for most tunnels contain conductors such as power cables strung along the lateral walls or under the roof, or rails, water pipes, etc. As will become evident in the next paragraphs, such conductors would change drastically the electromagnetic properties of the structure. In spite of the sometimes mediocre conductivity of the tunnel walls, we can already obtain a good picture of the propagation phenomena by comparing the tunnel with a hollow waveguide with highly conducting walls.

1.3.1. Simplified waveguide model

The theory of waveguides with perfectly conducting walls is available in numerous books, e.g. Marcuvitz (1951), and we will not develop it again here. We will only recall the main results as far as they have implications in the context of electromagnetic wave propagation in tunnels. The analysis is made for the harmonic time dependence $\exp(j\omega t)$. Theory resolves the electromagnetic field into a sum of solutions which are called modes. A mode is a solution with a dependence on the longitudinal coordinate z by a factor $\exp(-\Gamma z)$. The complex constant

$$\Gamma = \alpha + j\beta \qquad (1.5)$$

is the propagation constant of the mode. Its real part α is the specific attenuation expressed in Np/m and its imaginary part β is the specific phase shift or phase constant expressed in rad/m. The various modes obviously have different propagation constants and different field distributions.

For hollow waveguides with perfectly conducting walls the dependence of the propagation constant of a given mode on the frequency is very simple. Each mode is characterized by a critical frequency f_c which depends on the tunnel shape and size. Below this frequency the mode is evanescent, i.e. it suffers only attenuation and no phase shift : the specific attenuation is given by

$$\alpha = 2\pi\, f_c/c \left[1 - (f/f_c)^2\right]^{1/2} \qquad (1.6)$$

where $c = 3\ 10^8$ m/s is the speed of light. Above its critical frequency the mode propagates without attenuation and with a phase constant given by

$$\beta = 2\pi\, f_c/c \left[(f/f_c)^2 - 1\right]^{1/2} \qquad (1.7)$$

The mode having the lowest critical frequency is called the dominant mode and its critical frequency is called the waveguide cutoff frequency. Below this frequency all modes are evanescent and no electromagnetic energy can be conveyed by the waveguide.

The modes of a hollow waveguide with perfectly conducting walls are either transverse electric (TE) or transverse magnetic (TM), which means that either the electric or the magnetic field has no axial component. The dominant mode is always a TE mode. The modes are further labelled by a two-dimensional order number (m,n).

For a rectangular waveguide with cross-sectional dimensions a and b, the critical frequencies are given by

$$f_{cmn} = c/2 \left[(m/a)^2 + (n/b)^2\right]^{1/2} \qquad (1.8)$$

For TE modes m and n may be zero but not simultaneously, while for TM modes both must be strictly positive. Assuming that a > b, we see that the cutoff frequency is given by

$$f_c = f_{c10} = c/(2a) \qquad (1.9)$$

which means that the free-space wavelength at the cutoff frequency is twice the largest side of the rectangle.

For a circular waveguide with a radius a the critical frequencies are given by

$$f_{cmn} = \begin{cases} (cx_{mn})/2a & ; \quad \text{TM modes} \\ (cx'_{mn})/2a & ; \quad \text{TE modes} \end{cases} \qquad (1.10)$$

where $m \geq 0$; x_{mn} and x'_{mn} are the n-th zeros of the Bessel function $J_m(x)$ and of its derivative, respectively. The dominant mode is the TE_{11} mode. The critical frequencies of the six lowest-order modes are as follows

TE_{11} : 0.293 c/a	TE_{01} : 0.609 c/a
TM_{01} : 0.383 c/a	TM_{11} : 0.609 c/a
TE_{21} : 0.485 c/a	TE_{31} : 0.668 c/a

For tunnels of arbitrary shape, a very rough approximation is that the cutoff frequency is such that the free-space wavelength at this frequency is about equal to the tunnel perimeter and also that, well above the cutoff, the number of propagating modes grows as the square of frequency. The cross-section of most tunnels has dimensions of a few meters and the cutoff frequencies are consequently of a few tens of MHz. Below the tunnel cutoff the specific attenuation predicted by (1.6) is extremely high, say 1 dB/m or more, and no radio communication seems possible over appreciable ranges.

The model of a tunnel with perfectly conducting walls considered up to now is of course highly idealized. The most immediate effect of a finite conductivity is to introduce some attenuation of the modes above their respective critical frequency. In the case of metallic waveguides such as those used at microwave frequencies, the wall conductivity is nevertheless very high and the skin depth into the walls is extremely small when compared with the waveguide cross-section. This allows to calculate an approximate solution by a perturbation method. We will not recall the formulas obtained by this method for the specific attenuation of the modes above their respective critical frequency in a waveguide with highly conducting walls, since they can be found in any textbook on waveguides, namely Marcuvitz (1951). They are not applicable in most subsurface propagation problems. Indeed as the last column of Fig. 1.1 indicates, above the tunnel cutoff i.e. at a few tens of MHz, the ratio f/f_t is larger than unity for most tunnel wall materials. The latter then behave more as a lossy dielectric rather than as a conductor.

1.3.2. Comparison with experimental results

In spite of the expected weakness of the simple waveguide model, Deryck (1979) has nevertheless obtained a fairly good agreement between some experimental results and calculations based on formulas derived from the perturbation method. Figure 1.3 shows his results for the Lanaye tunnel, near Liège in Belgium. This tunnel is dug in calcareous tufa. It is 1600 m long, 5 to 6 m high and 4 to 5 m wide. The rock overburden is about 50 m thick. The value of the wall conductivity was obtained from a measurement of the attenuation of wave propagation through the rock and was found equal to 0.01 mho/m at 30 MHz. The tunnel has a flat floor and a round roof : it can be compared with a circular cylinder with a radius of 2.5 m, for which the cutoff frequency is 35 MHz.

The crosses on Fig. 1.3 show the measured values of the specific attenuation. Curve 2 shows the theoretical attenuation of a waveguide with perfectly conducting walls below the cutoff, while line 1 shows the attenuation for through-the-rock propagation. Theoretical attenuation curves above the cutoff obtained from the perturbation method are also drawn in solid lines. Deryck's conclusion is that the experimental results are for each frequency in accordance with the theoretical curve which predicts the lowest attenuation. This conclusion should not be considered as general. A counterexample in which the highest predicted attenuation is selected below cutoff will be found below.

The comparison of the measurements with the theoretical curves above the cutoff should also be used carefully. Indeed the steady decrease of the TE_{01} mode attenuation with frequency is a unique property of the circular waveguide and does generally not exist for other cross-sectional shapes. A theoretical calculation based on the perturbation method and taking into account that the tunnel floor is flat would probably not predict such a decrease.

Figure 1.4 shows results obtained by the same author for a rectangular road tunnel. The width of this tunnel was 17 m and the height 4.9 m. The tunnel walls were made of concrete. The cutoff frequency is 8.8 MHz. The dominant TE_{10} mode has a vertical polarisation. The measurements of the specific attenuation for this polarisation are represented by circles and agree fairly well with the theoretical prediction for the dominant mode up to about 200 MHz. The theoretical curve in solid line was again calculated by the perturbation method for a conductivity of 0.1 mho/m. This value seems somewhat high compared with the data of Fig. 1.1, but

it may be justified by the existence of concrete reinforcement. The TE_{mo} modes with m > 1 have not been taken into consideration although their critical frequencies are relatively low, being the multiples of 8.8 MHz. They should indeed not change the conclusions since their specific attenuation is always higher than that of the dominant mode. The waveguide model considered up to now can thus not explain the decrease of the measured attenuation above 200 MHz.

Measurements were also made by Deryck for the horizontal polarisation. The results are represented by crosses on Fig. 1.4 and they are compared with the theoretical attenuation curve in solid line for the TE_{01} mode. This mode is the lowest-order mode with horizontal polarisation in a waveguide with perfectly conducting walls. The measurements agree very well above the critical frequency (30.6 MHz) of this mode but fail completely below it. The discrepancy might be explained if some cross-polarising effect could be invoked, but this seems unprobable because the tunnel walls were very smooth. Instead we propose a different explanation that is supported by a more rigorous approach. If the wall conductivity is finite the modes are perturbed and their polarisation is slightly changed. The vertically polarized TE_{mo} modes now have a small component with horizontal polarisation and it is not surprising that the measured specific attenuation for the horizontal polarisation is the same as for these modes, since all modes with nominal horizontal polarisation are cutoff. The specific attenuation however does not tell everything and, to be complete, we also need to consider the coupling of the mode to the antenna, i.e. the absolute level of the field for a given transmitter power. Between 10 and 40 MHz this level should normally be significantly lower for the horizontal polarisation than for the vertical one. Indeed, Deryck confirmed that he observed a difference of 15 dB.

The reader could object that, if this explanation is correct, the vertical polarisation must propagate above 70 MHz with the specific attenuation of the TE_{01} mode rather than with the higher attenuation of the TE_{10} mode, because the former has a component with vertical polarisation. That this is not observed by Deryck can easily be explained. For the measuring distance used by this author the TE_{mo} modes, which are excited at a higher level by a vertical antenna, remain dominant in the measurement up to about 200 MHz in spite of their higher attenuation. At higher frequencies however the attenuation becomes so high that the vertical component of the TE_{om} (and other) modes dominates at the end of the measurement path : as a result the measured attenuation of the vertical polarisation tends to

that of these modes. This discussion shows how delicate the interpretation of experimental results can be.

On Figs 1.3 and 1.4 we have also drawn broken curves showing theoretical results based on an improved version of the perturbation approach. The main characteristics of results obtained in this way is that the theoretical curves have a horizontal asymptote for high frequencies. We cannot say that a better fit with the experimental data is obtained.

We may conclude that the simple waveguide model may give relatively good predictions of the attenuation up to a few times the cutoff frequency but that it needs to be refined. Theoretical and experimental investigations that will be reported in a later chapter show that, at higher frequencies, the specific attenuations decrease as f^{-2}. The simple waveguide model used hereabove thus fails completely at these frequencies.

1.3.3. Natural propagation above the cutoff

As the specific attenuation of the waveguide modes takes on relatively low values above the cutoff, it seems possible to communicate into tunnels without supplementary infrastructure. In this process the antennas of the radio sets are coupled to the electromagnetic field of the waveguide modes. Apart from the location and characteristics of the equipments no fundamental difference can be made here between a fixed base station and a mobile radio set. This type of communication based on natural propagation has unfortunately a limited application field because of several characteristics that we will examine briefly.

The decrease of the specific attenuation with frequency above the cutoff is rather slow. On the other hand, in many applications, it is not wanted to have a marked polarisation effect because the orientation of the mobile antennas may be arbitrary. These reasons are in favour of frequencies higher than say two or three times the cutoff. The existence of several propagating modes however has some drawbacks. These modes have different phase constants and their relative phases vary along a path parallel to the tunnel axis. As it is impossible to excite a single mode, the resulting standing waves are unavoidable in natural propagation. They show nodes which may be extremely deep. In cases where any breakdown of the communication link is dommageable, as in data transmission, it may be necessary to resort to suitable techniques like frequency or space diversity, error control, etc.

In speech transmission on the contrary some loss of communication may be tolerated. As the width of the deep standing waves nodes is minute, not exceeding a small fraction of the wavelength, this effect is acceptable for mobile communications. It is however necessary to take a safety margin such that good communications are obtained at a large percentage of places. When numerous modes with comparable amplitudes exist, the standing wave pattern looks random and the statistics of the field amplitudes tends to a Rayleigh distribution. The margin, defined as the ratio of the amplitudes exceeded at 1 % and x % of the places, amounts for this distribution to 16.4 dB, 19.5 dB and 26.6 dB for x = 90, 95 and 99 respectively.

Another important drawback in natural propagation is the disastrous effect of obstacles present in the tunnel. This is best understood if the propagation is viewed in terms of geometrical optics rather than by a decomposition into modes. It can be shown that both approaches are equivalent well above the tunnel cutoff. Geometrical optics decomposes the transmission between two antennas as a sum of a direct ray and of numerous rays which undergo reflections on the tunnel walls. Obviously an obstacle present in the tunnel will intercept some of the rays. This may suppress rays which have an unfavourable phase for a given receiving location and the standing wave pattern will thus be changed. However the main effect of an obstacle is to absorb a part of the energy, thereby creating a global loss. Indeed, the rays incident on the obstacle are partly reflected and partly refracted into the latter. The energy of the refracted rays is absorbed if the obstacle thickness is important compared with the skin depth. Most of the reflected rays emerge toward the nearby tunnel wall on which they fall with arbitrary incidence angles : remembering that the reflection is quasi-total only for those rays which have a grazing incidence, we see that a large part of the power scattered by the obstacle toward the tunnel walls will be absorbed into them.

This dependence of the reflection coefficient on the incidence angle allows us to predict qualitatively the effect of an obstacle in a straight tunnel wall above the cutoff. If the cross-section is clear, the rays contributing effectively to the received signal have a grazing incidence. If we admit that the energy of the rays intercepted by the obstacle is completely lost, we arrive at the conclusion that the power loss is equal to the ratio of the tunnel and obstacle cross-sections.

The effect of a curvature of the tunnel axis may be analysed by similar methods. Experience has shown that, in the UHF and higher bands, no communication can be established with receivers located in the shadow zone beyond a bend if the total distance exceeds about 100 m. It can easily be understood from geometrical optics considerations that sharp bends are more disastrous.

The limiting case is that of an abrupt corner. No ray from the geometrical approach can reach a receiver located beyond the corner and the only received signal comes from the wedge diffraction and subsequent reflections on the tunnel walls. A complementary and instructive picture is provided by physical optics. The cross-section of the transverse tunnel is illuminated by the sum of the incident wave and of the wave reflected by the corner into the main tunnel. As this sum is a standing wave with a phase change of 180° per half wavelength, the power transmitted to the transverse tunnel shows a global decrease with the ratio of the tunnel width to the wavelength. This evolution is oscillatory, the transmitted power showing deep minimums when this ratio is an integer number, separated by maximums at the half integer values. Similar considerations apply to the transmission in the main and transverse tunnels of a crossing or for the penetration of waves from open air into a tunnel.

As an example we will give some results obtained in an iron mine. The tunnels had a width of 7 m and a height of 8 m. The total attenuation between two antennas separated by a distance d with n corners could be written in the form (Delogne, 1976)

$$a = a_o + \alpha_d + nc + s \qquad \text{(dB)} \qquad (1.11)$$

where a_o is the standing wave envelope extrapolated to a zero distance, α is the global specific attenuation, c is the attenuation due to a corner and s is a margin for 95 % of the places. The measured values of these parameters are shown in table 1.1 and can be interpreted at the light of the previous discussion.

From these remarks we may conclude that diffraction effects play an important role in natural propagation in tunnels. Because of the general decrease of the specific attenuations, the highest frequency is undoubtedly the best choice for straight and unobstructed tunnels, but when corners and crossings exist, the best performance will be obtained in the 70 to 150 MHz band. The useful propagation ranges will nevertheless rarely exceed about 250 m when corners are present.

TABLE 1.1

f (MHz)	a_o dB	s dB	α dB/100 m	c dB
36	17	5	60	6
68	20	10	40	2
150	21	15	35	15
450	24	22	15	25

1.4. THE MONOFILAR MODE

The existence of a cutoff frequency in an empty tunnel and the very adverse effects of obstacles and bends on natural propagation at higher frequencies suggest to remove the cutoff effect by stringing an axial isolated wire conductor in the tunnel cross-section. The tunnel thereby becomes similar to a two-wire transmission line, the conductors of which are the wire and the tunnel wall. In addition to the waveguide modes the structure can then support a TEM-like transmission line mode which has no cutoff. It has been called coaxial mode in some early papers, because of the resemblance of the transmission line made by the tunnel and the wire to a coaxial cable, but the name monofilar mode is now generally accepted. As the specific attenuation of transmission lines in general increases with frequency, it is expected that this system will allow the use of relatively low frequencies propagating with a rather low specific attenuation.

Figure 1.5 may give a good though very approximate idea of the main properties of the monofilar mode. As shown, the transmission line current flows along the monofilar wire conductor and returns along the wall. The lines of the electric field are shown as continuous lines. Fixed base stations will be galvanically connected between the wire and the ground, while mobile transceivers will be coupled to the electromagnetic field of the monofilar mode.

In a practical installation, gauge considerations will not allow the radioelectrician to string the monofilar wire in the middle of the tunnel cross-section, but close to the wall. Such an eccentric location has an unfavourable effect for two reasons which appear clearly on Fig. 1.5. In the first instance the return current is no longer distributed more or less uniformly around the tunnel periphery but it tends to concentrate in those parts of the wall which are close to the wire. Things happen as if the cross-section of the return conductor was reduced. In transmission line terms the resistance of the return conductor is increased and this yields an increase of the specific attenuation of the monofilar mode. This dependence of the specific attenuation on the distance from the wire to the wall and on the frequency is evidenced by the measurements made by Deryck (1973, 1979) in the Lanaye tunnel and shown on Figure 1.6.

The other effect of an eccentric location of the monofilar wire is that the field lines and the electromagnetic energy tend to be concentrated between the wire and the proximate wall. The result is that portable radiosets located somewhere in the middle of the tunnel cross-section of near the opposite wall will only be weakly coupled to the monofilar mode. This effect can be expressed by an eccentricity loss which may in some cases amount to 30 to 40 dB. This is a very serious drawback, for this loss has to be substracted from the maximum allowable loss : once for base station-to-mobile and twice for mobile-to-mobile communication links.

The picture of the monofilar mode given by Fig. 1.5 and the subsequent discussion of the properties of this mode are valid for a highly conducting wall, i.e. wall below the transition frequency and provided the skin depth into the wall is much smaller than the tunnel cross-section and than the distance from the wire to the wall. This last condition is in most cases not satisfied and the previous conclusions are thus only qualitative.

An example where this qualitative picture fails was observed in salt and potash mines. In spite of the very low conductivity of the wall material the specific attenuation of the monofilar mode was significantly lower than for more conductive walls, which is somewhat surprising. The paradox can easily be explained however. As the skin depth into the wall is very large, the return current of the monofilar mode is distributed in a large area around the tunnel cross-section, whatever the monofilar wire location. The specific resistance of the return path, which is the dominant source of the specific attenuation, is the inverse product of this large

area by the conductivity. It is thus independent on the wire location and may be lower than for a very eccentric location in a more conductive tunnel. For the same reason the eccentricity effect will be less marked in such cases. From the discussion of this rather exceptional situation, it appears that a low wall conductivity, but also the use of low frequencies, may have advantages when the monofilar wire conductor must be strung very close to the tunnel wall.

In many practical situations, axial conductors exist in the tunnel, e.g. power lines, trolley wires, water pipes, etc. These conductors are in general not suitable to guide electromagnetic waves with a low specific attenuation, because they may contain longitudinal impedances or connections to the ground at radio frequencies. It will thus be necessary to string a dedicated monofilar wire conductor to support the monofilar mode. However if n axial conductors exist in the tunnel, there will be n TEM-like modes. Any discontinuity along such a structure creates inadvertent mode conversions and results in some loss. This effect as well as the field distribution of the useful mode are dependent on the relative locations of the monofilar wire and of the other conductors and may be reduced by a proper design. On the other hand, and on the contrary of what happened for the waveguide modes, transversal conductors and other obstacles present in the tunnel have few influence on the monofilar mode.

This enumeration of problems shows that, although the general characteristics of the monofilar wire technique are fairly simple, its use requires some experience and skill. A better knowledge of the theoretical aspects of the monofilar mode propagation is also needed.

1.5. THE LONG INDUCTION LOOP

A large induction loop installed around a building is sometimes used for paging applications. A similar technique may be used in mines. In the particular case of a tunnel the loop wire is strung near to opposite walls. The length-to-width ratio of the loop is much larger than unity and the loop perimeter is frequently larger than one wavelength. The structure thus operates as a transmission line rather than as a common induction loop and we will consider it from this point of view. Base stations are connected galvanically to the transmission line, while mobile transceivers are coupled to the magnetic field of the transmission line by means of a loop or ferrite antenna. The transmission line is terminated into

its characteristic impedance to avoid standing waves. As will become obvious from the discussion, the use of this technique is restricted to frequencies below a few hundreds of kHz.

As was stated in the previous section, the structure can support two TEM-like modes. If the two wires are perfectly symmetric with respect to the tunnel cross-section, these are the classical balanced and unbalanced modes. In the latter the transmission line current flows in equal parts along the two wires and returns along the tunnel wall. In the former the current flows along one wire and returns along the other one, while the tunnel wall carries no net longitudinal current.

For this reason, one should expect the balanced mode to have a much lower specific attenuation than the unbalanced mode. That this is not true can be seen by comparing Fig. 1.7 with 1.5. Because of the close proximity of the transmission line wires with the tunnel wall, the interwire capacity is much smaller than the wire-to-wall capacity, which means that there is a very weak coupling between the wires. The balanced and unbalanced modes can thus be seen as twice the monofilar mode existing for a single wire, with opposite and equal phases, respectively. Although no net current flows in the wall for the balanced mode, there is nevertheless a total current since the opposite-phase monofilar mode current distributions only partly cancel each other. If no cancellation occurs at all, the balanced and unbalanced modes have both the same specific attenuation as the monofilar mode of a single wire, as can be seen easily from Fig. 1.7. Theoretical calculations (Mahmoud, 1974a) confirm this trend. We made measurements of the specific attenuation of the balanced mode in the Lanaye tunnel below 1 MHz. The wires were strung at 50 cm from the wall. The results are shown on Figure 1.8 and are in fairly good agreement with those of Fig. 1.6 extrapolated below 1 MHz.

This tendency is reinforced when exact symmetry of the two wires cannot be maintained. The usefulness of the long induction loop is thus not much better than that of a monofilar wire.

1.6. LEAKY FEEDERS

1.6.1. Principle

The term leaky feeder covers a variety of open or semiopen transmission lines. Historically the first leaky feeder has been the two-wire ribbon feeder which is

very popular as an antenna feeder in television reception. When such a transmission line is strung parallel to the axis of a tunnel, we have a structure analog to the long induction loop with a balanced and an unbalanced mode. However the situation will be very different because the wire spacing is very small compared with the distance to the tunnel wall. As the electromagnetic field of the balanced mode decreases roughly as the square of the distance from the observation point to the transmission line, this mode induces negligible currents into the wall and, thereby, its propagation parameters, including the specific attenuation, will not differ from those of the transmission line in free space. The counterpart is that this mode is not directly useful for radio communications in the tunnel because it provides an extremely weak coupling to the antennas of mobile transceivers. The unbalanced mode has the inverse properties and does not differ much from the monofilar mode of a single wire located at the same place as the transmission line. This is why the balanced and unbalanced modes have been called the bifilar and monofilar modes, respectively, in the leaky feeder technique.

To understand why such a transmission line can improve radio communications in the tunnel, we must remember that strictly balanced and unbalanced modes cannot exist independently unless the two wires are perfectly symmetrical with respect to the tunnel wall. Any local asymmetry converts some energy from the one into the other. If such asymmetries are numerous, the monofilar mode will be regenerated by the bifilar mode and will exhibit an apparent specific attenuation equal to that of this mode, with a slight increase due to the mode conversion process. This seems to be an interesting principle for establishing long range radio communications in tunnels, for it promises the coupling properties of the monofilar mode with the low specific attenuation of the bifilar mode.

The ribbon feeder has however a very severe drawback. Its specific attenuation increases rapidly when it is covered with dust or moisture. To obviate this, several coaxial cables with an imperfect shield have been designed. Some of them are shown on Figure 1.9. The plastic jacket surrounding the cable provides a good protection against the penetration of moisture into the cable and, as a very large part of the power is confined under the shield, the transmission line mode is not seriously affected by a layer of dust and moisture on the external surface of the cable. From a practical viewpoint this is a sufficient reason to devote more attention to the coaxial leaky cables than to the ribbon feeder. Another and maybe more important characteristic of coaxial leaky feeders is the fact that the leakage field does not decrease as the square of the distance but rather as the distance itself.

A fundamental question in relation with leaky coaxial cables is how to characterize the transfer of electromagnetic energy through the imperfect shield. We will report some theoretical approaches to this very difficult problem. For most structures however, with the exception of the axial-slot cable, and for moderate frequencies, the imperfect shield can be modelized by a transfer inductance that will be noted m_t. This parameter relates the axial electric field on the shield surface E_z and the current carried by the latter by the equation

$$E_z = j\omega m_t I$$

The measurement of the transfer inductance requires some care but can easily be made in the laboratory (Krögel, 1956). For this purpose a short section of coaxial cable is fixed inside a metal tube of equal length to make a triaxial structure. The coaxial cable is fed at one end by a generator and terminated into its characteristic impedance. At the generator end the metal tube is closed by a metal plate which is soldered to the cable shield. At the other end, although this is not strictly necessary, the tube is carefully connected to the cable shield through the characteristic impedance of the coaxial cable consisting of the tube and shield. The voltage V appearing on this load is measured and the transfer impedance is obtained by $Z = V/(Id)$, where I is the generator current and d is the length of the structure. which must be very short compared with the wavelength. At low frequencies the transfer impedance may comprise a resistive part, which is the specific resistance of the shield, but at higher frequencies the imaginary part ($j\omega m_t$) should be dominant. Typical values of the transfer inductance of leaky coaxial cables range from 1 to 40 nH/m.

1.6.2. Leaky feeders below the tunnel cutoff

We have briefly explained in the previous section how the ribbon feeder works as a leaky feeder. Things are somewhat different for leaky coaxial cables. Again the structure can support two TEM-like modes. The first one is the perturbed transmission line mode and will be referred to as the coaxial mode. Some authors also use the name bifilar mode. It has the main part of its energy confined under the cable shield but with some leakage outside it. As far as this leakage remains weak, the power dissipated into the tunnel wall remains small and the specific attenuation does not differ much from that of a well shielded coaxial cable with the same characteristics. The second mode is called the monofilar mode and has just the inverse properties. It uses essentially the cable shield and the tunnel wall as conductors but has some leakage under the cable shield. Its specific attenuation is

not very different from that of a single wire transmission using a monofilar wire conductor instead of the leaky cable.

As was briefly mentioned in the previous section, leaky coaxial cables exhibit an important difference when compared with a ribbon feeder. For the latter, assuming a perfect symmetry with respect to the tunnel wall, the two wires carry exactly equal but opposite currents for the balanced or bifilar mode; no net current flows along the transmission line and this is why the electromagnetic field decreases as the square of the distance from the observation point to the transmission line. This does not remain exactly true if the two wires are not symmetrical with respect to the tunnel wall; however obtaining a noticeable asymmetry requires the ribbon feeder to be located very close to the tunnel wall. In a leaky coaxial cable on the contrary, the two conductors are intrinsically asymmetrical. Consequently the coaxial mode current which flows along the inner conductor returns mainly along the shield, but also partly along the wall. The transmission line thus carries a net current, with the result that the leakage field has a slower decrease with the distance from the observation point to the cable. The distribution of the coaxial mode leakage field in the tunnel cross-section is in fact that a monofilar mode travelling at the same velocity as the coaxial mode. In practice, below the tunnel cutoff, this distribution will not differ greatly from that of the main field of the monofilar mode. Inversely the leakage field of the monofilar mode inside the coaxial cable has approximately the same distribution as the main field of the coaxial mode (Delogne, 1975).

This behaviour of the leakage fields is of fundamental importance in the use of leaky coaxial cables. Indeed any source located on one side of the shield must necessarily excite both modes, though at different power levels. For instance, if a generator is connected at the input of the cable, nearly all the power will be delivered to the coaxial mode but the monofilar mode will also be excited. It can be shown (Delogne, 1976) that the initial power levels are such that the leakage field of the coaxial mode into the tunnel space is equal to the field of the monofilar mode. The specific attenuation for the latter is however in most applications several times higher than for the former and, at some distance from the generator, the leakage field of the coaxial mode is the dominant part of the electromagnetic field in the tunnel space. This example shows that the coaxial mode leakage is the mechanism used for base station to mobile communications, while the monofilar mode is here useless.

In mobile to mobile communications the transmitter excites the monofilar mode at a higher level than the coaxial mode and the leakage of the latter in the tunnel space will become dominant only at a rather large distance. There is no simple answer to the question wether the monofilar or the coaxial mode are the mechanism used in a long distance mobile to mobile communication : this depends on a number of factors.

1.6.3. Leaky feeders above the tunnel cutoff

Well above the cutoff frequency of the tunnel the working principle described hereabove fails. The monofilar mode has a specific attenuation which is much higher than that of the waveguide modes and it is therefore not very useful. On the other hand, the leakage field of the coaxial mode no longer has the same distribution as the monofilar mode and plays another role.

To understand this, let us first consider a leaky feeder strung into free space. This is basically a slow wave structure and consequently (Collin and Zucker, 1969) it does not radiate unless discontinuities are introduced along it. But as it comprises two conductors, it can support two slow waves having no cutoff. The first one is the coaxial mode, with the main part of the energy confined under the cable shield but with some leakage outside it. Its phase constant β_c is approximately given by

$$\beta_c = k_o \sqrt{\kappa} \qquad (1.12)$$

where κ is the dielectric constant of the cable insulating material. The second mode has the opposite energy distribution. It is a sort of Goubau wave with leakage under the cable shield; its phase constant lies typically in the range

$$\beta_g = k_o \ldots 1.02\ k_o \qquad (1.13)$$

depending on the cable jacket thickness and dielectric constant.

The field of both modes outside the cable can be expanded in cylindrical harmonics by a formula of the type

$$\sum_{m=o}^{\infty} A_m \begin{matrix}\sin\\ \cos\end{matrix} m\phi\ K_n(up) \qquad (1.14)$$

where $n = m$ or $(m + 1)$ according to the field component considered; K_n is the

modified Bessel function of the second kind and

$$u = (\beta^2 - k_o^2)^{1/2} \qquad (1.15)$$

The asymptotic formula for large t

$$K_n(t) \approx \left[\pi/(2t)\right]^{1/2} e^{-t} \qquad (1.16)$$

shows that the fields outside the cable are practically confined in an effective radius given by

$$\rho_e = 1/u \qquad (1.17)$$

Practical values of ρ_e for both modes are given in table 1.2 for a cable with $\kappa = 1.6$, $\beta_c = 1.26\ k_o$ and $\beta_g = 1.005\ k_o$.

TABLE 1.2

f (MHz)	ρ_{ec} (m)	ρ_{em} (m)
30	2.05	15.90
100	0.62	4.77
150	0.41	3.18
450	0.14	1.06

Any discontinuity along this structure will produce some mode conversion, but also radiation in the sense of a continuous spectrum of spherical waves. A generator connected at the cable input has a similar effect, exciting both guided modes but also radiation.

Let us now assume that this cable is strung in a tunnel. In most practical cases, the effective radius of the Goubau wave is larger than the distance between the cable and the wall and this wave becomes the classical monofilar mode with a somewhat modified field distribution. If a generator is connected to the cable input, the excited monofilar mode and radial radiation (or waveguide modes) are rapidly damped and there remains only the coaxial mode. Now, if the distance between the cable and the wall is larger than ρ_{ec}, this mode is virtually unaffected by the tunnel. Consequently, an observer located outside the effective radius will receive an extremely weak signal. Thus the cable does not radiate.

But if the wall comes into the effective radius of the coaxial mode, all wall irregularities and inhomogeneities will cause radiation. This is the only reason why leaky feeders radiate. It is a random process by nature. Note that the cable attachments produce a similar effect. It can be shown that if the scattering points are numerous and statistically independent, the field follows a Rayleigh distribution : indeed it is the result of the addition of numerous elementary contributions with random phases.

It has become common practice in the leaky feeder techniques at VHF and UHF to characterize the cable radiation by a coupling loss; this quantity is usually defined as the ratio of the power of the coaxial mode to the power received by a dipole antenna located at a specified distance from the cable. As the radiated field is random, the coupling loss should be specified as a value which is not exceeded at a certain percentage of places. In tunnel applications the coupling loss does not depend much on the distance from the receiving antenna to the cable.

As results from this discussion the coupling loss is an experimental parameter; it depends on a number of factors among which are the distance from the cable to the tunnel wall, the roughness of the latter, the mounting hardware, the frequency and, of course, the cable characteristics. It is thus not desirable to deviate significantly from the recommended mounting instructions of a leaky coaxial cable without proceeding to some measurements.

It is obvious that a strong radiation requires an important interaction between the coaxial mode leakage and the wall irregularities and cable attachments. These objects are not very efficient radiators and the process of diffraction and radiation necessarily involves an increase of the coaxial mode specific attenuation. To give an order of magnitude of this effect at 450 MHz, a coupling loss smaller

than 95 dB at 99 % of places currently yields a doubling of the cable attenuation; this is a very severe drawback. This theory was indeed fully confirmed by a campaign of measurements made in the subways of Paris : it was observed that a leaky cable no longer radiated at 450 MHz when it was strung at about 30 cm from the tunnel wall using thin nylon strings; at the same time the specific attenuation, which was doubled when the cable was against the wall, came back to the value of an equivalent non-leaky cable. A further conclusion of this analysis is that no particular leaky cable structure offers definite advantages for the use well above the tunnel cutoff; the only difference between the various types of cables, apart from internal parameters like the specific attenuation, is the relative intensity of the leakage; this can however be compensated by a suitable mounting.

1.7. MODE CONVERTERS

In the leaky feeder technique the transfer of energy from inside the cable to the tunnel space occurs continuously. In contrast with this method, it is possible to use a well-shielded coaxial cable along which discrete mode converters are inserted with a regular or irregular spacing. In such a cable the coaxial mode propagating inside the cable and the monofilar and waveguide modes propagating outside it are obviously completely independent. Creating a local energy exchange between the latter and the former thus requires to open the shield in some way.

In the first system of this kind, which has frequently been called INIEX/Delogne system because it was proposed by the author as a consultant of the Belgian Institut National des Industries Extractives (INIEX), the opening is an annular slot consisting of a complete interruption of the cable outer conductor. Refined theories of the working of such a slot are available (Delogne and Liegeois, 1971 - Wait and Hill, 1975d, 1975e). Below the tunnel cutoff however, a simplified quasi-static analysis of the slot can be obtained by considering the cable and the tunnel as two imbricated transmission lines having a common conductor. The latter is interrupted over a short length. The problem thus reduces to a circuit calculation which is suggested by Figures 1.10.a and 1.10.b, whereon Z_m and Z_c are the characteristic impedances of the monofilar and coaxial modes, respectively. The only fundamental difficulty in this respect is to define and estimate the value of Z_m. Fortunately it appears that this quantity varies slowly with the electrical and geometrical parameters of the structure. A comparison with the exact

electromagnetic solutions available between 1 and 50 MHz has shown that calculations based on the value of 377 ohms for Z_m never yields an error above 1 dB for the mode conversion factor.

A naked slot, like the one shown on Fig. 1.10, does not provide a good impedance match and a low insertion loss for the coaxial mode. Indeed, the external load impedance $2Z_m$ "seen" by the slot is rather high and most power flowing in the coaxial mode is reflected back inside the cable. As the objective of the system is to make use of the low specific attenuation of the coaxial mode to extend the range, it is necessary to improve the impedance match and to reduce the insertion loss to a very small value. This can be obtained by adding some lumped circuit elements to the slot. Various circuits may be used and will be described later.

This system has been used intensively in the HF band and at lower frequencies. The mode converter is in general designed to convert about 10 per cent of the power from the coaxial mode into the monofilar mode, which is paid by an insertion loss of a few tens of dB for the coaxial mode. This spacing between the mode converters is typically of several hundred meters. This technique provides an excellent flexibility in the design of a system because the mode converters parameters and spacing can be varied along the path in function of the tunnel cross-section, acceptable cable location, distance to the base station and so on. The only delicate point in the design task is to estimate the characteristics of the monofilar mode, namely the specific attenuation and the eccentricity loss; however an optimistic calculation, as well as changes due to the evolution of the underground workings, can still be corrected in situ by inserting additional mode converters.

Above the tunnel cutoff the slot will also excite the waveguide modes or, equivalently, natural propagation. It appears that the slot can be considered as an antenna fed by a part of the coaxial mode power. The radiation pattern has of course rotational symmetry about the cable axis. It exhibits a strong maximum at about 10 degrees of this axis, which is an excellent characteristic to launch natural propagation in the tunnel. The antenna gain in this optimum direction amounts to about 10 dB.

Another type of mode converter or radiator, according to the frequency range, is obtained by inserting a short length of a leaky cable into a well-shielded coaxial cable. This device has very similar characteristics to the annular slot, with an additional directional property. Mode converters have also been designed for the bifilar line.

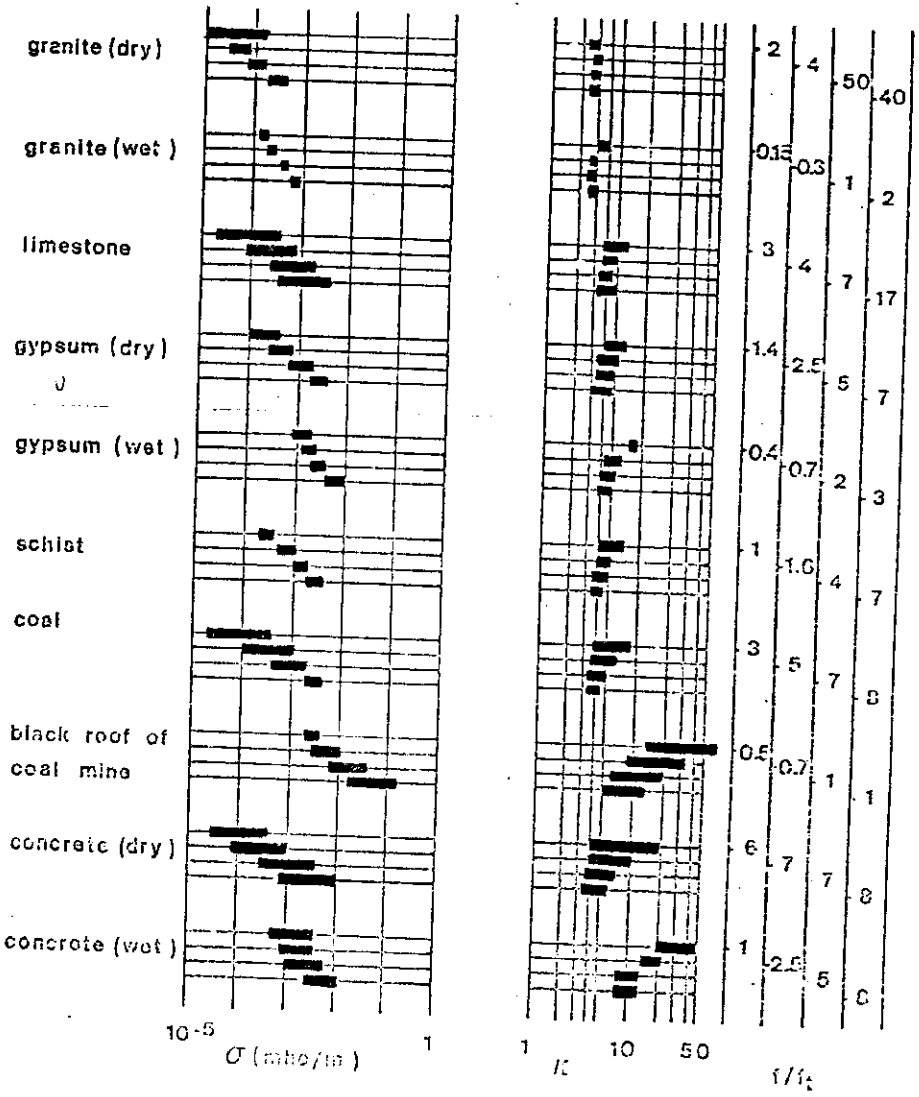

Fig. 1.1 Electrical parameters of some materials. For each material the heavy bars are from top to bottom for the frequencies of 1, 5, 25 and 100 MHz.

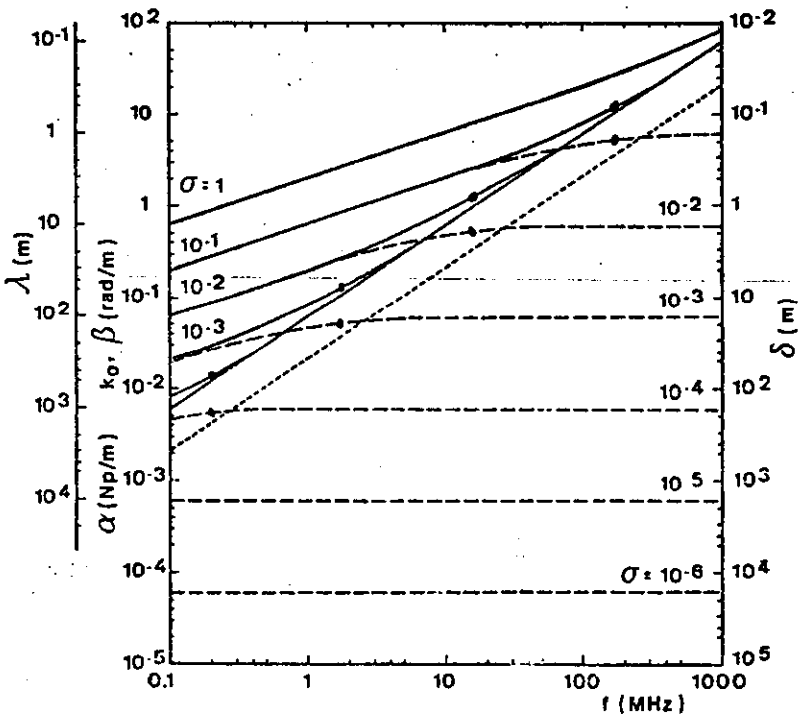

Fig. 1.2 Propagation parameters of a medium with dielectric constant $\kappa = 10$. Solid lines show β and λ. Broken lines are for α and δ. The dotted line is for the free-space wave number k_0. The dot on the α and β curves shows the transition frequency.

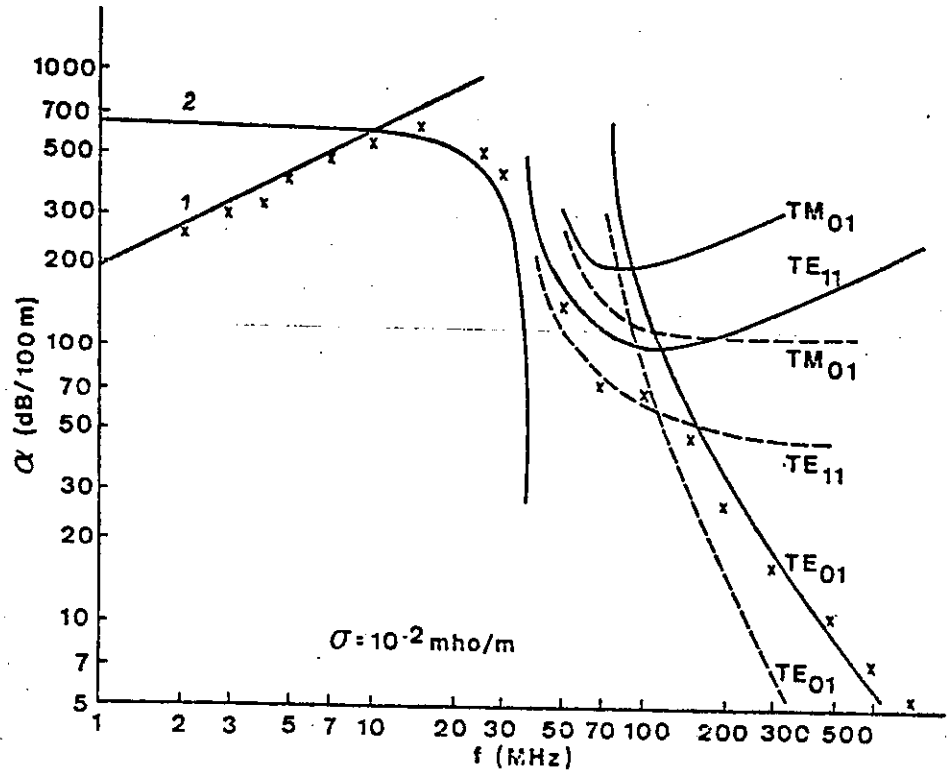

Fig. 1.3 Measured and calculated specific attenuation of natural propagation in the Lanaye tunnel.

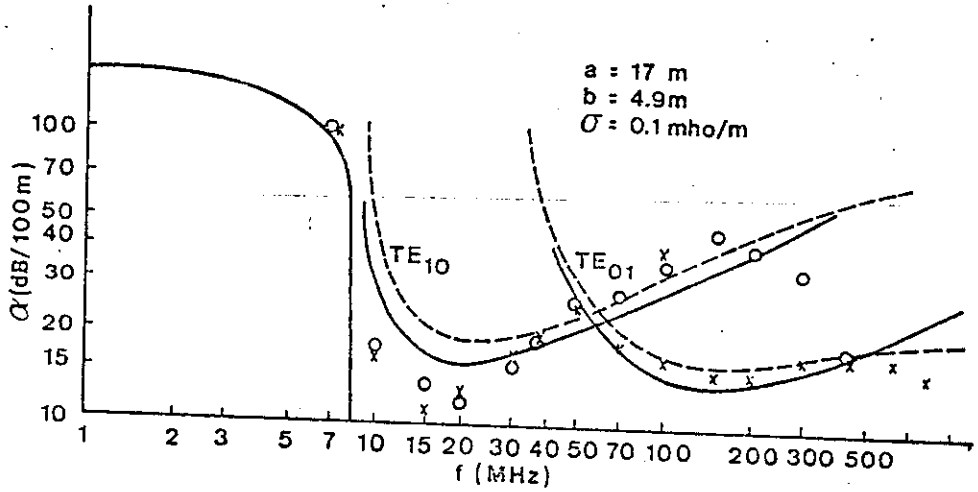

Fig. 1.4 Measured and calculated specific attenuation of natural propagation in a rectangular road tunnel. Circles are for vertical polarisation and crosses for horizontal polarisation.

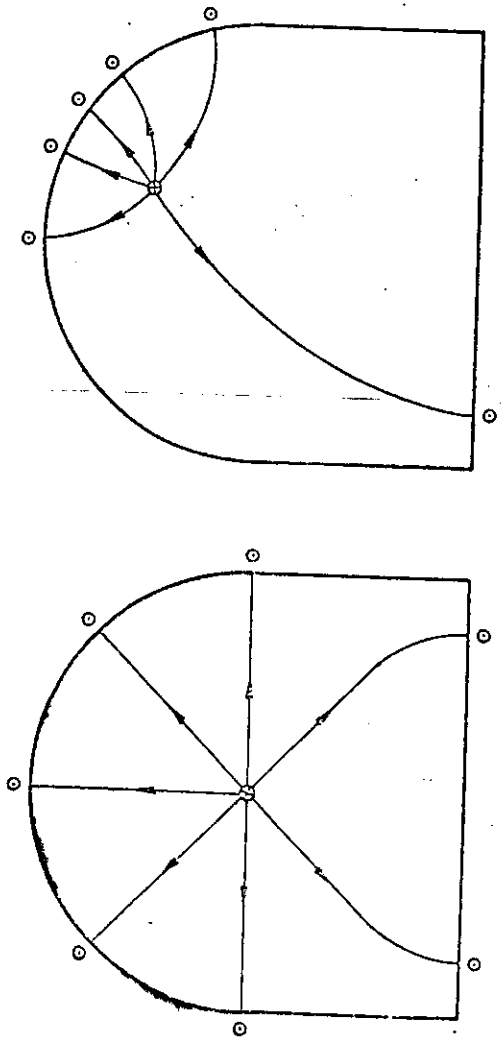

Fig. 1.5 Current distribution and electric field lines of the monofilar mode.

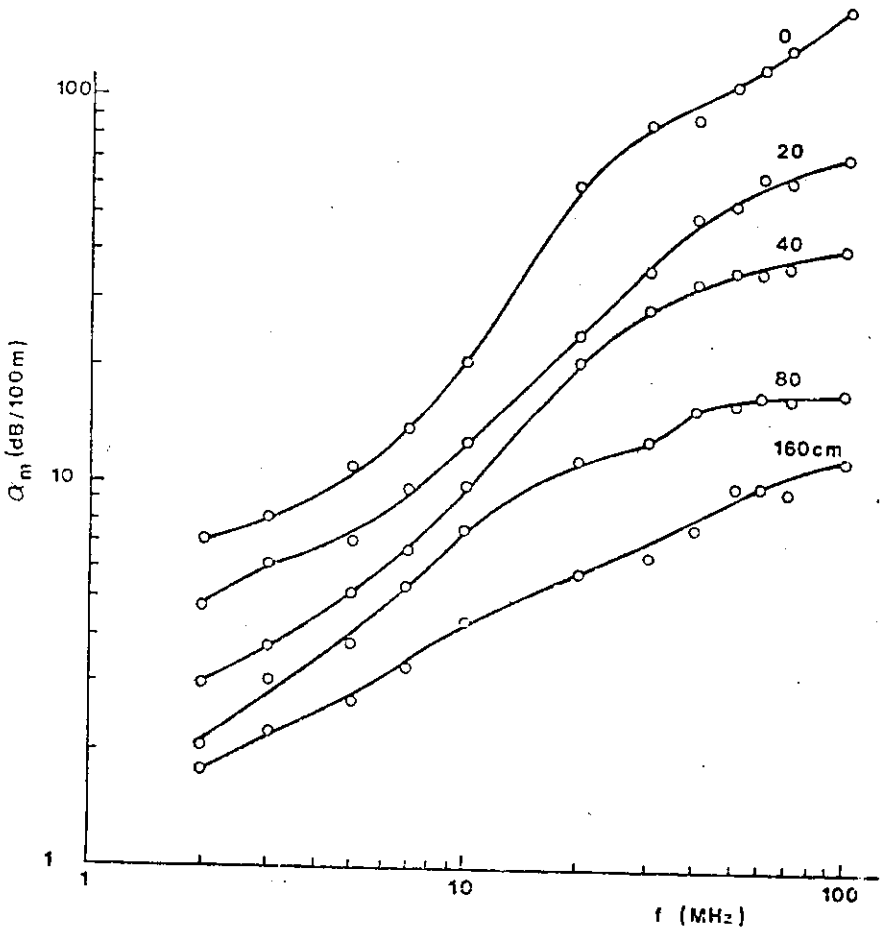

Fig. 1.6 Measured specific attenuation of the monofilar mode in the Laneye tunnel as a function of frequency and distance from the cable to the tunnel wall.

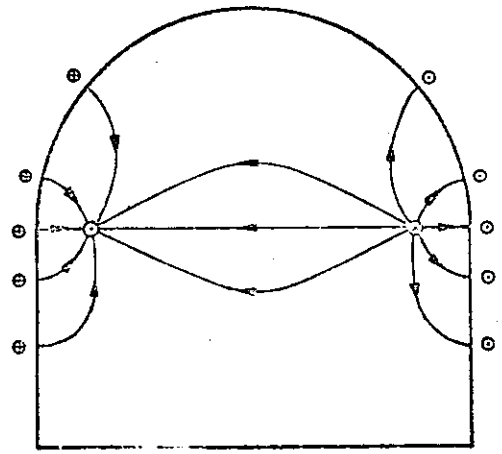

Fig. 1.7 Current distribution and electric field lines for the long induction loop.

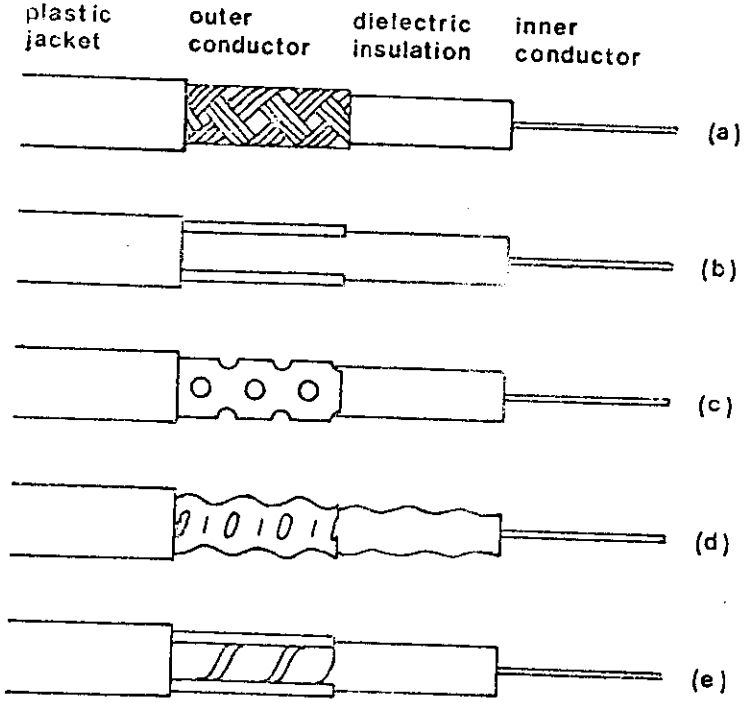

Fig. 1.5 Some leaky coaxial cables : (a) loosely braided (b) longitudinal slot (c) perforated tube (d) helically formed and grinded (e) helical tape and longitudinal slot.

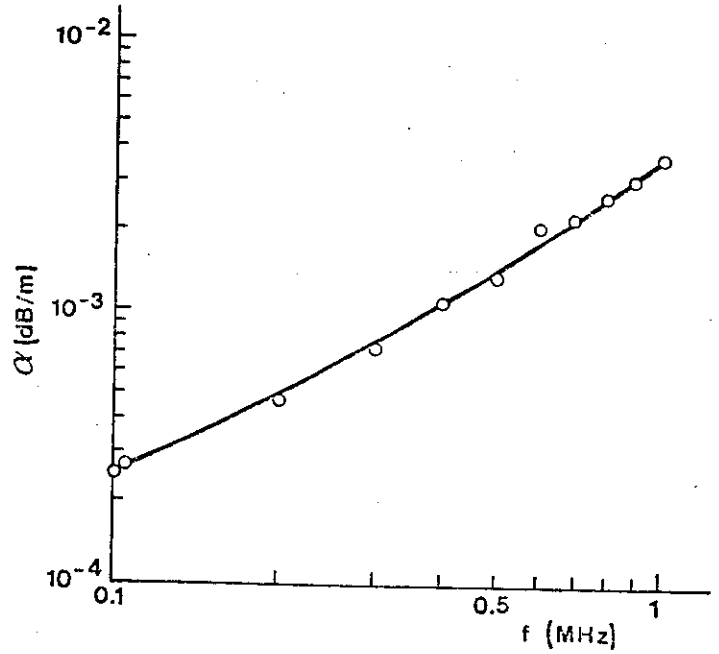

Fig. 1.6 Specific attenuation of a long induction loop in the Lenaye tunnel.

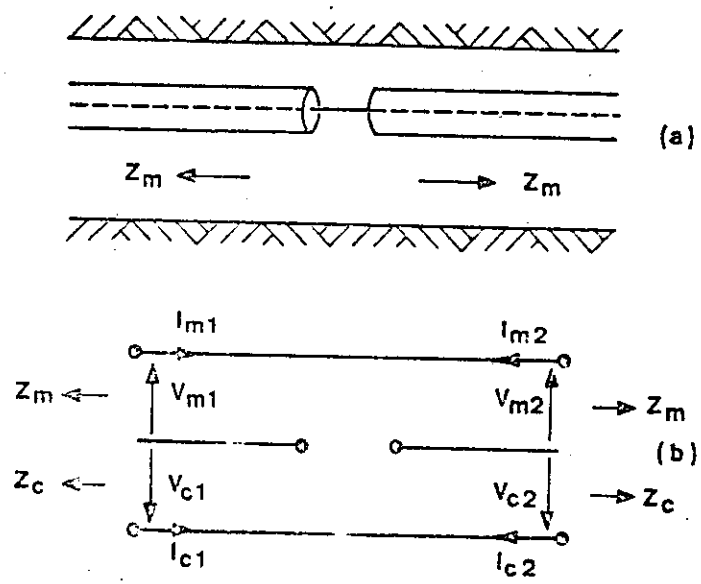

Fig. 1.10 Principle of the annular-slot mode converter : (a) pictorial view, (b) equivalent circuit.

CHAPTER 2 ELECTROMAGNETIC THEORY OF SUBSURFACE PROPAGATION

2.1. INTRODUCTION

In this chapter we will state and solve the electromagnetic problem associated with propagation in some idealized subsurface cylindrical structures. The term cylindrical means that the geometrical and electrical parameters of the medium do not depend on a coordinate z which is in most cases the distance along the axis of a tunnel. Although the structures considered here are highly idealized compared with actual subsurface environments, the related electromagnetic problem is among the most sophisticated. The reason for this is that we have to do with at least two media, one of which has a finite conductivity. Consequently simple solutions consisting for instance of transverse electric (TE) or transverse magnetic (TM) waves cannot generally match the boundary conditions. In many cases all the six scalar components of the electric and magnetic field are non-zero.

The main problem which will be investigated here is to solve Maxwell's equations

$$\text{curl } \bar{E} = j\omega \mu_o \bar{H} - \bar{J}_{ma} \qquad (2.1)$$

$$\text{curl } \bar{H} = (\sigma + j\omega \varepsilon_o \kappa) \bar{E} + \bar{J}_a \qquad (2.2)$$

wherein the following notations are used :

$\bar{E}$, $\bar{H}$: electric, resp. magnetic field

μ_o = $4\pi \cdot 10^{-7}$ permeability of the medium, assumed to be equal in all cases to that of free space

ε_o = 8.85 . 10^{-12} free space permittivity

σ , κ : conductivity and dielectric constant of the medium, respectively

$\bar{J}_{ma}$, $\bar{J}_a$: applied magnetic, resp. electric current densities.

We will use a complex dielectric constant ε defined by

$$j\omega \varepsilon = \sigma + j\omega \varepsilon_o \kappa \qquad (2.3)$$

The complex propagation constant γ, complex wave number k and intrinsic impedance η of the medium are defined by

$$\gamma = jk = (j\omega \mu_o \cdot j\omega \varepsilon)^{1/2} \qquad (2.4)$$

$$\eta = \omega \mu_o / k \qquad (2.5)$$

The term "applied" used for the current densities $\bar{J}_{ma}$ and $\bar{J}_a$ means that they are considered as given, i.e. as the source of the electromagnetic field. The reader who is not familiar with this formulation will point out that magnetic currents do not actually exist. This is undoubtedly true. A reason for using applied magnetic currents is that some electric current distributions may be replaced by an equivalent but simpler magnetic current density. For instance a small loop of area dA and unit normal $\bar{n}$ carrying a current I is equivalent to a magnetic Hertz dipole of moment (Stratton, 1941)

$$I_m \, d\bar{s} = - j\omega \mu_o \, I \, dA \, \bar{n} \qquad (2.6)$$

The form (1)-(2) of Maxwell's equations is valid in a homogeneous medium. The structures considered in this chapter are a juxtaposition of homogeneous media and these equations apply to each of them provided the appropriate values of σ and κ are used. Uniqueness theorems require some boundary conditions to be satisfied at the interface of different media and to infinity. Specifically the tangential components of the electric and magnetic fields must be continuous at an interface.

Boundary conditions to infinity sometimes require a detailed discussion. It is obvious that in any physically realizable solution, sources of electromagnetic fields are located at a finite distance and, as the external medium considered in this chapter has always a finite non-zero conductivity, that the solution of Maxwell's equations must vanish to infinity in all directions. However we will frequently be concerned with propagation modes of a cylindrical structure. Propagation modes are solutions of sourceless ($\bar{J}_{ma} = 0$, $\bar{J}_a = 0$) Maxwell's equations with a dependence on the longitudinal coordinate z expressed by a factor $\exp(-\Gamma z)$, where

$$\Gamma = \alpha + j\beta \qquad (2.7)$$

is the mode propagation constant, α and β being the specific attenuation and phase constants, respectively. If we assume that α is positive, which generally also yields β positive, the mode fields will be infinite for $z = -\infty$. Such solutions obviously assume that a source with infinite power exists to infinity in the negative direction of the z-axis. A fundamental question which raises here is to know whether or not we must impose these solutions to decrease to infinity in other directions than the negative z-axis. The answer to this question is positive, but is is known that modes violating this condition (improper modes) may in some cases accurately represent the actual fields in a finite region of space.

2.2. ELECTROMAGNETIC POTENTIALS

As was mentioned in the previous section, we will frequently be concerned with problems where all the six components of the electric and magnetic fields are non-zero. In such a situation electromagnetic potentials are extremely efficient mathematical tools. Instead of solving Maxwell's equations (2.1) and (2.2), we first calculate an electric-type Hertz vector potential $\bar{\pi}'$ and a magnetic-type Hertz vector potential $\bar{\pi}''$ satisfying the equations

$$\nabla^2 \bar{\pi}' + k^2 \bar{\pi}' = -(j\omega \varepsilon)^{-1} \bar{J}_a \qquad (2.8)$$

$$\nabla^2 \bar{\pi}'' + k^2 \bar{\pi}'' = -(j\omega \mu_o)^{-1} \bar{J}_{ma} \qquad (2.9)$$

The fields are then obtained by

$$\bar{E} = \text{curl curl } \bar{\pi}' - j\omega \mu_o \text{ curl } \bar{\pi}'' - (j\omega \varepsilon)^{-1} \bar{J}_a \qquad (2.10)$$

$$\bar{H} = \text{curl curl } \bar{\pi}'' + j\omega \varepsilon \text{ curl } \bar{\pi}' - (j\omega \mu_o)^{-1} \bar{J}_{ma} \qquad (2.11)$$

This is the most general representation of the electromagnetic fields using two vector-potentials. The reader may feel this formulation to be unnecessarily complicated because we still have to work with six scalar components and, in addition, intricate formules. One may indeed observe that $\bar{E}'$ and $\bar{H}''$ satisfy equations

$$\nabla^2 \bar{E}' + k^2 \bar{E}' = j\omega \mu_o \bar{J}_a \qquad (2.12)$$

$$\nabla^2 \bar{H}'' + k^2 \bar{H}'' = j\omega \varepsilon \bar{J}_{ma} \qquad (2.13)$$

and that it seems simpler to solve these equations directly. The usefulness of potentials results from the following statement, which is an extension of a theorem proved by Jones (1964) : *when, in some volume filled with a homogeneous medium, only z-directed electric and magnetic currents are applied, the electromagnetic fields can always be derived from z-directed electric and magnetic Hertz potentials.*

The above statement is extremely interesting for we shall always be concerned with cases where the applied electric or magnetic current densities, if any, are restricted to one cartesian component. It is then still possible to solve the problem using an electric-type and a magnetic-type Hertz potentials with one non-zero component along the same cartesian axis. Frequently there will be no applied current density at all. The choice of this axis is then free. In some cases it is also possible to use two cartesian components of the same, either electric or magnetic, potential or a component of $\bar{\pi}'$ and another component of $\bar{\pi}''$. There thus remains some freedom which can be used to simplify the mathematical analysis. In some simple problems it is even possible to find the solution using only one adequately selected scalar component. In order to facilitate the choice and the calculations, we have gathered in appendix A a complete set of formulas for the cartesian coordinate system. Appendix B contains formulas for the cylindrical coordinate system when the potentials π'_z and π''_z are used. These functions will frequently be denoted by

$$U = \pi'_z \quad , \quad V = \pi''_z \tag{2.14}$$

We will not dwell on a discussion of the 15 possible choices of a pair of scalar components, but formulate some useful observations. For interfaces parallel to the z-axis, if the pair (π'_z , π''_z) is used, the boundary conditions involve only these functions and their first derivatives. Moreover the continuity of E_z and H_z at these interfaces are uncoupled because π'_z and π''_z yield $H_z = 0$ and $E_z = 0$ respectively. This pair is thus of interest. Furthermore it is well adapted to the case of cylindrical coordinates. In some cases however, other pairs may be of interest too, but it must be stressed that this depends on the approach which is chosen to solve the problem.

2.3. THIN-CABLE APPROXIMATION

As we have seen in the first chapter, many systems developed to guide e.m. waves along tunnels involve cables or wires which are drawn parallel to the cable axis. An exact solution of the relevant e.m. problem would require to solve Maxwell's equations inside and outside the cable and to express boundary conditions at the cable surface. This is a titanic work, even in the simplest cases, and some simplifying assumptions are needed. Approximations are possible because the diameter of wires and leaky feeders used in subsurface radio communications is generally

much smaller than the distance from this cable to the tunnel wall and than the wavelength. These approximations also apply to other similar problems, like for wires or cables strung above the ground or buried in the latter.

The sketch of the analysis is as follows. Let us assume that a cable with radius ρ_1 is located along the z-axis of a cylindrical coordinate system (ρ,ϕ,z) and that we are studying a solution characterized by a propagation factor $\exp(-\Gamma z)$. We suppose that outside the cable, for $\rho_1 < \rho < \rho_2$, we have a homogeneous medium with a wavenumber denoted by k and we define the transverse wave number by

$$v = \sqrt{-k^2 - \Gamma^2} \tag{2.15}$$

It is possible to decompose the fields outside the cable into Fourier series of the type

$$(\bar{E},\bar{H}) = \sum_{m=-\infty}^{\infty} (\bar{E}_m,\bar{H}_m) \exp(jm\phi) \tag{2.16}$$

From the uniqueness theorem of electromagnetic theory it is known that the fields outside the cable are determined by the tangential components $E_{\phi m}(\rho_1)$ and $E_{zm}(\rho_1)$. It is interesting to investigate how the various field components for $\rho > \rho_1$ depend on the latter.

The discussion shows that in the limit of a vanishing cable radius, i.e. for $|v\rho_1| << 1$, and as far as we are interested in the calculation of the field in regions $\rho >> \rho_1$, only the rotational symmetric component $E_{zo}(\rho_1)$ of the electric field at the cable surface has a significant contribution. The rotational symmetric part $E_{\phi o}(\rho_1)$ and the asymmetric components $E_{\phi m}(\rho_1)$ and $E_{zm}(\rho_1)$ have a negligible influence. This assumption will be referred to as the *thin-cable approximation*. It obviously does not mean that the rotational asymmetric part of the field does not exist, even at the cable outer surface. In particular the medium or the sources located at $\rho > \rho_2$ may force these components to exist and in many cases to have comparable amplitudes for some values of ρ. We must however observe that it is possible to imagine cable structures which would imply a large value of the neglected term $E_{\phi o}(\rho_1)$, but this is generally not the case in leaky feeders.

The thin-cable approximation has the advantage that it reduces the study of the cable interior to searching a relation between the rotational symmetric parts

E_{zo}, $H_{\phi o}$ and H_{zo} at the cable outer surface. It completely disconnects the studies of the fields inside and outside the cable. This is a great simplification of the problem.

As can be expected for a cable carrying some longitudinal currents, it turns out in most cases that H_{zo} is zero or negligible and that the cable can be modelled by a surface impedance relation of the type

$$E_{zo}(\rho_1) = Z_o H_{\phi o}(\rho_1) \tag{2.17}$$

The quantity $I = 2\pi\rho_1 H_{\phi o}(\rho_1)$ will be referred to as the total current carried by the cable. Defining the *specific internal impedance*

$$z_o = \frac{Z_o}{2\pi\rho_1} \tag{2.18}$$

we may rewrite (2.17) as

$$E_{zo} = z_o I \tag{2.19}$$

Quite generally the surface impedance Z_o is not an intrinsic characteristic of the cable, for it depends on the external medium through the mode propagation constant Γ.

2.4. SURFACE IMPEDANCE OF A THIN CONDUCTING WIRE

We will now consider the simple case of a cable consisting of a conducting wire of radius c. In order to obtain the surface impedance, we need to concentrate on the electromagnetic field inside the wire, for which we use the following notations

$$\gamma_i = j\omega\mu\tilde{\sigma} \tag{2.20}$$

$$\tilde{\sigma} = \sigma + j\omega\varepsilon \tag{2.21}$$

$$w = \sqrt{\gamma_i^2 - \Gamma^2}\quad ,\quad \mathrm{Re}\ w \geq 0 \tag{2.22}$$

Note that we will not assume that $\mu = \mu_o$ for the wire material.

The solution of Maxwell's equations inside the wire is given by equations (B.18) to (B.24) of appendix B wherein we have to use w instead of u. The constants A_m and B_m must be zero to keep the fields finite on the wire axis. On eliminating the constants P_m and Q_m between (B.19) to (B.24), it can easily be shown that, anywhere inside the conducting wire, we have

$$E_{zm} = Z_{zzm} H_{zm} + Z_{z\phi m} H_{\phi m} \tag{2.23}$$

$$E_{\phi m} = Z_{\phi zm} H_{zm} + Z_{\phi\phi m} H_{\phi m} \tag{2.24}$$

where

$$Z_{zzm} = \frac{-jm\,\Gamma\rho\ I_m(w\rho)}{\tilde{\sigma}\rho\ w\rho\ I_m'(w\rho)} \tag{2.25}$$

$$Z_{z\phi m} = \frac{w\rho\ I_m(w\rho)}{\tilde{\sigma}\rho\ I_m'(w\rho)} \tag{2.26}$$

$$Z_{\phi\phi m} = \frac{jm\,\Gamma\rho\ I_m(w\rho)}{\tilde{\sigma}\rho\ w\rho\ I_m'(w\rho)} \tag{2.27}$$

$$Z_{\phi zm} = \frac{-(\gamma_i\rho)^2\ I_m'(w\rho)}{\tilde{\sigma}\rho\ w\rho\ I_m(w\rho)} + \frac{m^2(\Gamma\rho)^2\ I_m(w\rho)}{\tilde{\sigma}\rho\ (w\rho)^3\ I_m'(w\rho)} \tag{2.28}$$

As the boundary conditions at an interface require the continuity of the tangential components of the fields, these relations, wherein ρ is replaced by c, hold on the external surface of the wire. Hence we have obtained a surface impedance matrix for each cylindrical harmonic. This matrix depends on the mode propagation constant Γ through the transverse wave number w. This result is valid whatever the external medium and the sources located therein. We can now introduce some approximations.

As we explained in the previous section, in the thin-wire approximation, we are solely interested in the rotational symmetric element $Z_{z\phi o}$, denoted Z_o. This surface impedance is given by (2.26) with $m = 0$ and $\rho = c$. We may further assume that $|\Gamma| \ll \gamma_i$. This approximation is justified in all cases where the wire is a good conductor. A good conductor is indeed defined by the property

$$\sigma \gg \omega\varepsilon \tag{2.29}$$

which implies

$$\gamma_i = \frac{1 + j}{\delta} \tag{2.30}$$

where

$$\delta = \sqrt{\frac{2}{\omega\sigma\mu}} \qquad (2.31)$$

is the skin depth into the conductor. Our assumption is thus that the mode wavelength is much larger than the skin depth into the conductor material. In this case, $w = \gamma_1$ and (2.26) yields

$$Z_o = \frac{\gamma_1 c\, I_o(\gamma_1 c)}{\sigma c\, I_o'(\gamma_1 c)} \qquad (2.32)$$

This value has now become independent on the mode propagation constant. Two extreme cases may be considered. First, if the wire radius is small compared with the skin depth, $|\gamma_1 c|$ is a small quantity. Using the approximations

$$I_o(x) = 1 \qquad (2.33)$$

$$I_o'(x) = \frac{x}{2} \qquad (2.33)$$

for $|x| \ll 1$, we get the trivial static limit

$$Z_o = 2/(\sigma c) \qquad (2.34)$$

If, on the contrary, $|\gamma_1 c|$ is a large quantity, the use of the large-argument approximation

$$I_o(x) = \frac{e^x}{\sqrt{2\pi x}} \quad , \quad |x| \gg 1 \qquad (2.35)$$

yields

$$Z_o = \eta_1 \qquad (2.36)$$

where

$$\eta_1 = \sqrt{\frac{j\omega\mu}{\tilde{\sigma}}} = \sqrt{\frac{j\omega\mu}{\sigma}} \qquad (2.37)$$

is the intrinsic impedance of the conductor material. The specific external impedance is thus given by

$$z_o = \frac{\eta_1}{2\pi c} \qquad (2.38)$$

We now may comment somewhat further on the thin-wire approximation. As we have explained in the previous section, this approach is used in some applications

wherein the quantities of interest mainly depend on $Z_o = Z_{z\phi o}$. This does not mean that the other neglected surface impedances are much smaller than this quantity. As a proof of this statement, we may consider a conducting wire for which we have $|\Gamma| \ll \gamma_1$ and $|\gamma_1 c| \gg 1$. Then for all cylindrical harmonics for which $|\gamma_1 c| \gg m$, it is easy to show from (2.25) to (2.28) the

$$|Z_{zzm}| \cdot |Z_{\phi\phi m}| \ll |\eta_1|$$

$$Z_{z\phi m} = -Z_{\phi z m} = \eta_1 \qquad (2.39)$$

For these cylindrical harmonics, the surface impedance is thus isotropic and equal to Z_o.

2.5. TRANSFER PROPERTIES OF LEAKY FEEDERS

2.5.1. The transfer impedance concept

Coaxial cables have been used for the transmission of electromagnetic energy for many years. The screening effect of the outer conductor provides obvious advantages. Perfect shielding can be obtained by using a plain outer conductor provided the shield thickness is large compared with the skin depth into the conductor material. This condition cannot easily be fulfilled at low frequencies : skin depth into copper at 100 kHz is about 0.2 mm. Under such conditions, signals propagating inside the coaxial cable give rise to an axial voltage on the outer surface of the shield and are thereby coupled to the external space. The inverse process also occurs by reciprocity. In order to get a simple picture of the phenomenon, we may imagine that the cable is drawn parallel to a return path which may be referred to as the structural ground. The cable shield can then be seen as the common return path of two transmission lines. In the frame of the present study, these transmission lines convey what we have called the coaxial and monofilar modes.

As a current flowing inside the coaxial cable gives rise to an axial voltage in the outer transmission line and conversely, we expect to get coupled transmission lines of the type

$$-\frac{dV_c}{dz} = z_c I_c + z_t I_m \qquad (2.40)$$

$$-\frac{dI_c}{dz} = y_c V_c \qquad (2.41)$$

$$-\frac{dV_m}{dz} = z_m I_m + z_t I_c \qquad (2.42)$$

$$-\frac{dI_m}{dz} = y_m V_m \qquad (2.43)$$

where the subscripts c and m recall the names coaxial and monofilar, respectively.

Alternatively we may write equations (2.40) and (2.42) as

$$-\frac{dV_c}{dz} = (z_c - z_t)I_c - z_t I_s \qquad (2.44)$$

$$-\frac{dV_m}{dz} = (z_m - z_t)I_m - z_t I_s \qquad (2.45)$$

where

$$I_s = -(I_c + I_m) \qquad (2.46)$$

is the total current carried by the cable shield . t[illegible] direction of the z-axis. Equivalent circuits of a line element corresponding to the use of either (2.40)-(2.42) or (2.44)-(2.45) are shown on Figures 2.1.a and 2.1.b respectively. For completeness we have also shown a transverse coupling admittance y_t which is sometimes used, with a corresponding modification of eq. (2.41)-(2.43).

A cable shield is said to be *electrically thin* if the tangential electric field is continuous through the shield. For a plain shield this obviously requires the shield thickness to be small compared with the skin depth. For such shields, the circuit diagram of Fig. 2.1.b provides a simple physical interpretation of the impedance elements. According to this representation indeed, the axial voltage drop is the voltage which appears between points A and B. The axial electric field along the shield is given by

$$E_z = \frac{-(V_A - V_B)}{dz} = z_t I_s \qquad (2.47)$$

and the *specific transfer inductance* z_t appears to be the impedance of a unit length of the imperfect shield. Similarly $(z_c - z_t)$ and $(z_m - z_t)$ appear to be the specific series impedances of the inner and outer circuits in the hypothetic situation where the actual shield is removed and replaced by a perfect conductor.

For electrically-thick shields, Fig. 2.1 may remain valid but giving a physical interpretation to Fig. 2.1.b is not allowed. Indeed, points located on the inner and outer surfaces of the shield are not equipotential and we may not say that a point like B is actually common to the inner and outer circuits.

The model of coupled lines shown on Fig. 2.1 was first developed by Schelkunoff (1934) for coaxial cables with a plain but imperfectly conducting shield. In this case the model is not necessarily restricted to electrically thin shields. For practical reasons, namely mechanical flexibility, the shield of coaxial cables is frequently braided. It then contains numerous small apertures through which an additional leakage of electromagnetic energy can occur. In the leaky feeders like those shown on Fig. 1.9, this mechanism is deliberately enhanced.

As a first and rough approach to this problem, we will show that the apertures give rise to an additional inductive transfer impedance. For this purpose, let us consider a periodic distribution of apertures in an infinitely-thin conducting plane shield, as shown on Figure 2.2. We will assume that the aperture shape and location are symmetric with respect to the z-axis. We further suppose that the shield carries a mean current density K_{zo} in the direction of the z-axis and that this quantity does not depend on x. The lines of current are obviously distorted by the apertures, as shown on part (a) of the figure. Part (b) shows a magnified view of the reference aperture located at the origin of axes.

The current distribution induces a magnetic field which, by symmetry, has only a y-component inside the apertures. Let us assume that the current distribution $\overline{K}(x,z)$ is known and that $H_y(x,o,z)$ inside the reference aperture may be calculated from it by magnetostatic methods. This seems to be justified provided the period of the structure is small compared with the wavelength. Obviously $H_y(x,o,z)$ is an odd function of x and it is negative for $x > o$. Maxwell's equation

$$\text{curl } \overline{E} = -j\omega\mu_o \overline{H} \qquad (2.48)$$

shows that E_x and E_z are odd and even functions of x, respectively. As a result, the average value of the tangential electric field in the apertures is parallel to the z-axis. No tangential electric field can of course exist on the screen outside the apertures.

Let us now consider average values on one period of the structure. These quantities are defined by expressions like

$$\bar{f}_o = \frac{1}{A_p} \int_{\text{period}} \bar{f}\, dS \qquad (2.49)$$

where A_p is the area of one period. They are the zero-order terms of a two-dimensional Fourier series. We obtain in particular

$$K_{zo}\, \bar{u}_z = \frac{1}{A_p} \int \bar{K}(x,z)\, dS \qquad (2.50)$$

$$E_{zo} = \frac{1}{A_p} \int_{\text{aperture}} E_z\, dS \qquad (2.51)$$

Part of the last integral can be calculated by applying the integral form of (2.48) to the contour ABC of Fig. 2.2.b. As the electric field is normal to AB and BC, which run along a metallic surface, this yields

$$\int_C^A E_z(x,o,z)\, dz = -j\omega\mu_o \int_{ABC} H_y(x',o,z')\, dx'\, dz' \qquad (2.52)$$

This quantity has still to be integrated from $(-x_1)$ to x_1 to obtain the integral in the second part of (2.51). As the right-hand side of (2.52) is proportional to the average current density K_{zo}, this provides a relation of the type

$$E_{zo} = j\omega M_s K_{zo} \qquad (2.53)$$

On the other hand the average values of the magnetic field above and below the screen are tangential and x-oriented. They undergo a discontinuity given by

$$K_{zo} = H_{xo}(y - o) - H_{xo}(y + o) \qquad (2.54)$$

Equation (2.53) thus becomes a transfer condition for the electromagnetic fields :

$$E_{zo} = j\omega M_s \left[H_x(y - o) - H_x(y + o)\right] \qquad (2.55)$$

It can easily be seen that M_s is a positive quantity. It is called the ***surface transfer inductance***, while

$$Z_s = j\omega M_s \qquad (2.56)$$

is called the ***surface transfer impedance***, with respective units henries and ohms. If we make abstraction of the coordinate system, (2.55) may be written

$$\bar{E}_t = Z_s\, \bar{n}_2 \times \left(\bar{H}_{t2} - \bar{H}_{t1}\right) \qquad (2.57)$$

for a plane screen separating two media referred to by suscripts 1 and 2; here $\bar{n}_2$ is the unit normal to the screen, oriented toward medium 2.

We now can extend the concept of surface inductance to perforated coaxial-cable shields. As far as the size and period of the apertures are small compared with the shield radius b, we may expect that the fields near to the shield are not significantly modified by the curvature and that we have the same surface transfer inductance as for a plane shield. Equation (2.57) then becomes

$$E_{zo} = Z_s \left[H_{\phi o}(b + o) - H_{\phi o}(b - o)\right] \qquad (2.58)$$

The magnetic field discontinuity on the right-hand side of this equation is obviously related to the screen current I_s by

$$2\pi b \left[H_{\phi o}(b + o) - H_{\phi o}(b - o)\right] = I_s \qquad (2.59)$$

Combining these equations and comparing the result with (2.47) yields the ***specific transfer impedance***

$$z_t = \frac{Z_s}{2\pi b} \qquad (2.60)$$

which consists of a ***specific transfer inductance***

$$m_t = \frac{M_s}{2\pi b} \qquad (2.61)$$

These quantities have Ω/m and H/m as respective units.

If the size and lateral period of the apertures are not small compared with the shield radius, we may expect that relations of type (2.58) to (2.61) will still exist, but the transfer parameters can obviously no longer be obtained from those of a plane shield. It is also clear that, particularly in this case, the fields depart significantly from rotational symmetry. In some problems we may nevertheless restrict our interest to the rotational symmetric part, as we have seen in section 2.3.

The foregoing approach to the concept of transfer inductance has been made deliberately heuristic. To be really meaningfull the transfer impedance should be an intrinsinc parameter of the shield : it should be independent of quantities such as the internal parameters of the cable (dielectric constant of the insulator, diameter of the inner conductor) and of the external medium. Experimental (Krügel, 1956) and theoretical approaches (Wait, 1976b; Hill and Wait, 1980a,b; Delogne and Laloux, 1980) tend to show that this is true for most leaky feeder types. The transfer inductance of leaky feeder shields can be theoretically predicted with a fairly good accuracy. Practical values range from 3 to 30 nH/m.

2.5.2. External surface impedance of a leaky coaxial cable

According to the thin-cable approximation developed in section 2.3, the quantity which is needed to express boundary conditions at the outer surface of a leaky cable of radius b is either the external surface impedance Z_o defined by

$$E_{zo}(b + 0) = Z_o \, H_{\phi o}(b + 0)$$

or the specific external impedance

$$z_o = E_{zo}(b + 0) \; / \; \left[2\pi b \, H_{\phi o}(b + 0)\right]$$

We shall now calculate this parameter for leaky coaxial cables having a shield characterized by a specific transfer impedance $z_t = j\omega m_t$. Before defining exactly the internal structure of the cable, let us first look at a general problem. We study a wave characterized by a propagation factor $\exp(-\Gamma z)$ within a homogeneous medium located between the radii ρ_1 and ρ_2 of a cylindrical coordinate system. With the notations of Appendix B, we may write for the rotational symmetric fields in this region

$$E_{zo}(\rho) = - u^2 \, V_o(u\rho) \tag{2.62}$$

$$H_{\phi o}(\rho) = - j\omega\varepsilon u \, V_o'(u\rho) \tag{2.63}$$

with

$$V_o(u\rho) = Q \, I_o(u\rho) + B \, K_o(u\rho) \tag{2.64}$$

If this region is located inside a thin cable, i.e. if $|u\rho| \ll 1$, we may approximate this function and its derivative by

$$V_o(u\rho) = Q + B \ln \frac{C u\rho}{2} \tag{2.65}$$

$$V_o'(u\rho) = B/(u\rho) \tag{2.66}$$

where $C = 1.7810....$ Let us consider the quantity

$$z_o(\rho) = \frac{E_{zo}(\rho)}{2\pi\rho \, H_{\phi o}(\rho)} \tag{2.67}$$

We may write

$$\frac{2\pi j\omega\varepsilon \, z_o(\rho)}{u^2} = \frac{Q}{B} + \ln \frac{C u\rho}{2} \tag{2.68}$$

Considering two radii ρ_1 and ρ_2 and eliminating the ratio Q/B, we obtain the general relation

$$z_o(\rho_2) = z_o(\rho_1) + \frac{u^2}{2\pi j\omega\varepsilon} \ln \frac{\rho_2}{\rho_1} \tag{2.69}$$

This relation is very useful to obtain the external specific impedance of a leaky cable. The inner conductor, with conductivity σ and permeability μ, has a radius a. Then we have, according to eq. (2.38) :

$$z_o(a) = \frac{1}{2\pi a} \sqrt{\frac{j\omega\mu}{\sigma}} \tag{2.70}$$

If the cable insulation has a wavenumber k and a permittivity ε, we obtain

$$z_o(b - 0) = z_o(a) - \frac{k^2 + \Gamma^2}{2\pi j\omega\varepsilon} \ln \frac{b}{a} \tag{2.71}$$

If the specific transfer impedance of the shield is z_t, we may write eq. (2.58) and (2.59) as

$$\frac{1}{z_o(b + 0)} = \frac{1}{z_o(b - 0)} + \frac{1}{z_t} \tag{2.72}$$

Finally the shield may be coated by a dielectric layer with wavenumber k_c, permittivity ε_c and external radius c. We then have, using (2.69)

$$z_o(c) = z_o(b + 0) - \frac{k_c^2 + \Gamma^2}{2\pi j\omega\varepsilon_c} \ln \frac{c}{b} \tag{2.73}$$

Equations (2.70) to (2.73) may be represented by the ladder network of Figure 2.3, with

$$z_{ba} = -\frac{k^2 + \Gamma^2}{2\pi j\omega\varepsilon} \ln\frac{b}{a} \qquad (2.74)$$

$$z_{cb} = -\frac{k_c^2 + \Gamma^2}{2\pi j\omega\varepsilon_c} \ln\frac{c}{b} \qquad (2.75)$$

It is instructive to consider the value of the external specific impedance for a particular case. Let us assume that the internal conductor is perfectly conducting, that the specific transfer impedance consists of an inductance m_t and that there is no external coating. Remembering the expression of the specific inductance of a perfectly shielded cable

$$l_o = \frac{\mu_o}{2\pi} \ln\frac{b}{a} \qquad (2.76)$$

it is easy to show that

$$z_o(b + 0) = j\omega \frac{m_t\, l_o(1 + \Gamma^2/k^2)}{m_t + l_o(1 + \Gamma^2/k^2)} \qquad (2.77)$$

Neglecting the specific attenuation, $\Gamma = j\beta$, it is seen that the specific external impedance consists of a reactance. This reactance has a zero for $\beta = k$ and a pole for $\beta = k(l_o + m_t)/l_o$ and is a decreasing function of β. It is positive if the wave is faster than the TEM mode of the perfectly shielded cable ($\beta < k$) or if $\beta > k(l_o + m_t)/l_o$ and negative between these two limits.

2.6. NATURAL PROPAGATION IN A LOW-CONDUCTIVITY LAYER

Having prepared the required mathematical tools in the previous sections, we are now ready to study the propagation of electromagnetic waves in some subsurface structures. By natural propagation, we mean that there is no wire or leaky feeder specially installed to guide e.m. waves. The simplest of these structures is a plane layer of relatively low conductivity embedded between the two semi-infinite media of higher conductivity. This situation is characteristic of coal seams as we have in section 1.2. We will start with the analysis of some waveguiding properties of the layer and then consider the excitation of guided modes by elementary sources.

2.6.1. Guided plane waves

The geometrical and electrical parameters of the layer are defined on Figure 2.4. In this section, we are interested in plane waves, without dependance of the fields on x coordinate and with a dependence on y coordinate by a factor $\exp(-\Gamma y)$. These modes can be obtained from a z-oriented electric Hertz potential $\pi'_z = U(z)\exp(-\Gamma y)$, where U satisfies equation

$$\frac{d^2U}{dz^2} - u^2 U = 0 \qquad (2.78)$$

with

$$u = \sqrt{-k^2 - \Gamma^2} \qquad (2.79)$$

By convention, we use for u the square root with the determination

$$-\pi/2 < \arg u \leqslant \pi/2 \qquad (2.80)$$

The fields may be obtained by

$$E_y = -\Gamma \frac{dU}{dz} \qquad (2.81)$$

$$E_z = -\Gamma^2 U(z) \qquad (2.82)$$

$$H_x = -j\omega\varepsilon\, \Gamma\, U(z) \qquad (2.83)$$

where

$$j\omega\varepsilon = j\omega\varepsilon_o \kappa + \sigma \qquad (2.84)$$

All these quantities need to be used with subscripts 1 or 2 for the external half-spaces.

The solution of (2.78) yielding decreasing fields in the lower and upper half-speces if given by

$$U = \begin{cases} A\, e^{-u_1 z} & \text{for} \quad z > a \qquad (2.85a) \\ B\, e^{uz} + C\, e^{-uz} & \text{for} \quad 0 < z < a \qquad (2.85b) \\ D\, e^{u_2 z} & \text{for} \quad z < 0 \qquad (2.85c) \end{cases}$$

where A, B, C, D are arbitrary constants. These may be determined by requiring the continuity of E_y and H_x, i.e. of $\Gamma\, dU/dz$ and $k^2\, U$ at the interfaces. This yields a linear system of four homogeneous equations with four unknowns. The mode equation is obtained by expressing that the determinant of this system is zero.

With the notations

$$R_1 = \frac{k_1^2\, u - k^2\, u_1}{k_1^2\, u + k^2\, u_1} \tag{2.86}$$

$$R_2 = \frac{k_2^2\, u - k^2\, u_2}{k_2^2\, u + k^2\, u_2} \tag{2.87}$$

the mode equation is found to be

$$R_1\, R_2 = e^{2ua} \tag{2.88}$$

The quantity R_1 is recognized as the reflection factor of plane waves with a propagation factor $\exp(-\Gamma y - uz)$ on the interface $z = a$, while R_2 is relative to the interface $z = 0$. As u, u_1 and u_2 are even functions of the unknown Γ, the roots of this equation occur in opposite pairs $\pm \Gamma^{(0)}, \pm \Gamma^{(1)}, \pm \Gamma^{(2)} \ldots$, where by convention $-\pi/2 < \arg \Gamma^{(n)} \leq \pi/2$.

Before giving some numerical results, we would like to discuss some limiting cases. For perfectly conducting boundaries, k_1 and k_2 become infinite, the reflection factors R_1, R_2 tend to unity and the solutions of (2.88) are $ua = jn\pi$. The zero-order mode is the classical TEM mode of the parallel-plate waveguide. The specific attenuation of this mode is the same as for plane waves in an infinite space of conductivity σ and dielectric constant κ. The modes with $n \neq 0$ are the TM waveguide modes. They have critical frequencies which correspond to a seam thickness equal to n times the half-wavelength in this medium. Below this frequency they suffer a very high attenuation and above it the attenuation remains larger than that of the TEM mode. The latter has no critical frequency. It is clear that, when $|k_1| \gg k$ and $|k_2| \gg k$, the modes of the actual waveguide are similar to those of this limiting case. This occurs below the transition frequencies of the external media, i.e. for $\omega\varepsilon_o\, \kappa_1 \ll \sigma_1$ and $\omega\varepsilon_o\, \kappa_2 \ll \sigma_2$, provided $\sigma_1 \gg \sigma$ and $\sigma_2 \gg \sigma$. In the limiting case, the fields of the even (odd) modes are even (odd) functions of z in the seam and the TEM mode is independant on z.

As expected, the specific attenuation of the dominant zero-order mode increases with frequency. In actual subsurface propagation problems it takes acceptable values only below a few MHz. In this frequency range, the higher-order modes are below cut-off and are consequently useless. This is the main reason why we do not devote attention at present to the TE modes which all have critical frequencies.

The main field components of the TM modes are E_z and H_x with a slight longitudinal component. The transverse components are even (odd) functions of z for the even (odd) modes, at least for the limiting case or when the external media have the same characteristics.

Another limiting case occurs when the waveguide thickness tends to zero and when the external media are identical. It can be seen from (2.88) that we have then $u_1 = 0$. Consequently the specific attenuation of the dominant mode is equal to that of plane waves in the external medium. Actually when the waveguide thickness is small, the specific attenuation lies between that of the internal medium and those of the external half spaces.

Some values of the attenuation of the zero-order mode have been published (Wait, 1976a) for a coal seam embedded between two semi-infinite rock half-spaces having identical electrical parameters. We performed a systematic numerical analysis of this mode. Equation (2.88) has been solved by Newton-Raphson's iteration method for a wide choice of electrical parameters and for frequencies between 100 kHz and 100 MHz. From a theoretical point of view, it is interesting to note that, for some combinations of electrical parameters and frequency, it happens that no root is found, i.e. no guided mode exists. Specifically, when the conductivities σ and σ_1 are both very low, the zero-order mode disappears above a few MHz. This is not surprising since the coal and rock media are then lossy dielectrics ($\omega\varepsilon \gg \sigma$) rather than conductors and the coal seam height is much smaller than the wavelength.

For normal values of the rock conductivity however, the zero-order mode always exists. A first conclusion of this systematic analysis is that the rock dielectric constant κ_1 has a very limited influence on the mode propagation constant. Consecuently the value $\kappa_1 = 2\kappa$ has been used for all results presented below.

These results are shown on Figure 2.5.a to c for three seam heights a = 2, 4 and 8 m, two values of the coal dielectric constant κ = 4 and 9, and two values of the rock conductivity σ_1 = 0.1 and 0.01 mho/m. Six curves are shown on each diagram : the five lower curves, from bottom to top, give the mode attenuation for conductivity ratios σ_1/σ of 5000, 1000, 500, 100 and 50, and the upper curve gives the attenuation of plane waves in the rock medium.

Comments of the results are as follows. Below a frequency corresponding roughly to the cutoff of the first-order mode, i.e. when the seam height is smaller than half the wavelength in coal, the attenuation of the zero-order mode increases with frequency and, to some extent, with the resistivity of the coal medium. It may be verified that the attenuation is most frequently much higher than that of plane waves in an infinite coal medium. This is not surprising, particularly at the low frequency end of the curves : since the skin depth into the rock medium is large, attenuation mainly occurs in this medium. Actually, obtaining a mode attenuation close to that of plane waves in coal requires a high rock conductivity rather than a high value of the ratio σ_1/σ. The dependence of the mode attenuation on the coal conductivity is reduced when frequency increases.

As expected the attenuation varies inversely with seam thickness. The curves suggest that relatively low attenuations can be obtained at high frequencies for thick seams. The reader should however keep in mind the evolution of the electrical parameters of natural media with frequency as shown on Figure 1.1.

2.6.2. Excitation by a vertical electric dipole

Waves with vertical polarisation can be excited by a vertical electric dipole. We thus consider such a dipole with moment Ids located at a height z_o on the z-axis within the low-conductivity seam of Figure 2.4. The problem is mathematically similar to the radiation of a vertical electric dipole located between a flat earth and the ionosphere. The solution is available (Wait, 1976), but we will derive it with some detail since the principle of the approach that will be used is a powerful tool for the solution of several subsurface propagation problems. This will allow us to be more concise in the following sections.

The method used here consists of first calculating the radiation of the dipole in an infinite homogeneous space and then of modifying this result to account for reflection and refraction at the interfaces. The solution of the first problem

yields the primary fields. Using a vertical electric Hertz potential, we have

$$\pi_z^{(p)} = M \exp(-jkR/R) \tag{2.89}$$

where R is the distance to the dipole and

$$M = \frac{Ids}{4\pi j\omega\varepsilon} \tag{2.90}$$

This is a very classical result. However it is not in the adequate form since spherical coordinates are ill-suited to the geometry of our problem. Cartesian or cylindrical coordinates are undoubtedly preferable.

We may imagine the electric dipole as a surface current density applied on an elementary cylinder of vanishing radius ρ_o and of height ds. Then, according to eq. (2.8), the primary potential satisfies equation

$$\left[\frac{\partial^2}{\partial\rho^2} + \frac{1}{\rho}\frac{\partial}{\partial\rho} + \frac{\partial^2}{\partial z^2} + k^2\right]\pi_z^{(p)}(\rho,z) = \frac{-Ids}{2\pi j\omega\varepsilon\rho_o}\,\delta(\rho - \rho_o)\,\delta(z - z_o) \tag{2.91}$$

This equation can easily be solved by applying a Fourier transform to the z-coordinate and using the Green's function eq. (C.11) of Appendix C. Finally ρ_o is allowed to vanish. The solution is obtained in the form

$$\pi_z^{(p)} = \frac{Ids}{2\pi j\omega\varepsilon}\int_C H_o^{(2)}(\lambda\rho)\,\frac{\exp(-jh|z-z_o|)}{jh}\,\lambda\,d\lambda \tag{2.92}$$

where h is related to λ by

$$h = (k^2 - \lambda^2)^{1/2} \tag{2.93}$$

with the determination

$$-\pi < \arg h \leq 0 \tag{2.94}$$

for this square root. The integration path C in the complex λ plane is shown on Figure 2.6.

The result (2.92) is classical. It can be traced back to Sommerfeld. The primary potential is now in an adequate form to start with the analysis of the dipole re-

diation in the low conductivity seam. The secondary potential $\pi_z^{(s)}$ is due to multiple reflection and refraction of the primary potential at the interfaces $z = 0$ and $z = a$. In each of the media $z < 0$, $0 < z < a$ and $z > a$, it satisfies an equation of the type (2.91), but without a source term and with the adequate value of k. This homogeneous equation can be solved by a similar Fourier transform technique. Consequently, after the same manipulations, we may write the secondary potential in the form

$$\pi_z^{(s)} = \frac{Ids}{2\pi j\omega\varepsilon} \begin{cases} \int_C H_o^{(2)}(\lambda\rho)\, A(\lambda)\, e^{-jh_1 z}\, \frac{\lambda d\lambda}{jh_1} & \text{for } z > a \\ \int_C H_o^{(2)}(\lambda\rho) \left[B(\lambda)\, e^{jhz} + C(\lambda)\, e^{-jhz}\right] \frac{\lambda d\lambda}{jh} & \text{for } 0 < z < a \\ \int_C H_o^{(2)}(\lambda\rho)\, D(\lambda)\, e^{jh_2 z}\, \frac{\lambda d\lambda}{jh_2} & \text{for } z < 0 \end{cases} \tag{2.95}$$

where h_1 and h_2 are defined as functions of λ by

$$h_1 = \sqrt{k_1^2 - \lambda^2} \quad ; \quad -\pi < \arg h_1 \leq 0 \tag{2.96}$$

$$h_2 = \sqrt{k_2^2 - \lambda^2} \quad ; \quad -\pi < \arg h_2 \leq 0 \tag{2.97}$$

and A, B, C, D are still unknown functions of λ. The arbitrary choice of determinations (2.96) and (2.97) has been duly taken into account in eq. (2.95) to satisfy the boundary conditions to infinity.

The unknown functions are to be determined from the boundary conditions at the interfaces. The continuity of the tangential field components requires that the total potential satisfies the conditions

$$k^2\pi_z(a - 0) = k_1^2\, \pi_z(a + 0)$$

$$\frac{\partial\pi_z(a - 0)}{\partial z} = \frac{\partial\pi_z(a + 0)}{\partial z} \tag{2.98}$$

$$k^2\pi_z(-0) = k_2\pi_z(-0)$$

$$\frac{\partial\pi_z(+0)}{\partial z} = \frac{\partial\pi_z(-0)}{\partial z} \tag{2.99}$$

Since these conditions are to be met for all values of ρ, they may be expressed directly for the integrands of (2.92) and (2.95).

The algebraic calculations to obtain the unknown functions are lengthy, but straight-forward. We define the reflection factors of the interfaces by

$$R_1(\lambda) = \frac{k_1^2 h - k^2 h_1}{k_1^2 h + k^2 h_1} \tag{2.100}$$

$$R_2(\lambda) = \frac{k_2^2 h - k^2 h_2}{k_2^2 h + k^2 h_2} \tag{2.101}$$

and obtain

$$B(\lambda) = -e^{-jhz_o} + \frac{e^{-jhz_o} + R_1\, e^{-jh(2a - z_o)}}{\Delta}\, e^{jha} \tag{2.102}$$

$$C(\lambda) = -e^{jhz_o} + \frac{e^{jhz_o} + R_2\, e^{-jhz_o}}{\Delta}\, e^{jha} \tag{2.103}$$

$$A(\lambda) = \frac{k^2(1 + R_1)}{k_1^2 R_1}\, C(\lambda) \tag{2.104}$$

$$D(\lambda) = \frac{k^2(1 + R_2)}{k_2^2 R_2}\, B(\lambda) \tag{2.105}$$

$$\Delta(\lambda) = e^{jha} - R_1 R_2\, e^{-jha} \tag{2.106}$$

Note that the expressions of the reflection factors are identical to (2.86) and (2.87) with the substitutions $u = -jh$, $u_1 = -jh_1$, $u_2 = -jh_2$, $\Gamma = j\lambda$.

Hence we concentrate on the region $0 < z < a$ only. The total potential may now be written

$$\pi_z(x,y,z) = \frac{M}{2j} \int_C H_o^{(2)}(\lambda\rho)\, \frac{F(\lambda)}{\Delta(\lambda)}\, \frac{\lambda d\lambda}{h} \tag{2.107}$$

where

$$F(\lambda) = \left[e^{jhz_<} + R_2\, e^{-jhz_<}\right] \left[e^{jh(a - z_>)} + R_1\, e^{-jh(a - z_>)}\right] \tag{2.108}$$

and $z_<$ and $z_>$ denote the smallest and the largest of the heights z and z_o, respectively.

The integral (2.107) can be evaluated by function theoretic methods. In order to do this, we need to identify the singularities of the integrand in the λ-plane (Figure 2.6). In the first instance we note that the Hankel function is two-valued; the reason for this is the existence of a logarithm function in the definition of the Neumann function $N_o(\lambda\rho)$. Consequently a branch cut must be drawn along the negative real axis. The integration contour C must run below this branch cut. The functions $h_1(\lambda)$ and $h_2(\lambda)$ defined by (2.96) and (2.97) are also two-valued. According to the chosen determinations, we must draw branch cuts corresponding to the forbidden boundaries arg $h_1 = \pi$ and arg $h_2 = \pi$. It can be seen that these branch cuts are parts of the hyperboles passing through the points of affixes $\pm k_1$ and $\pm k_2$ and having the real and imaginary axes as asymptotes. Actually the branch cuts are those parts of the hyperbolas that run along the imaginary axis. The definition (2.94) of h also requires a branch cut. However it can be seen that the integrand of (2.107) remains unchanged if h is replaced by (-h) : this results of (2.100), (2.101), (2.106) and (2.108) considered as function of h. Consequently the two-valued character of h is not maintained for the integrand of (2.107) and the branch cut is immaterial.

Furthermore the integrand of (2.107) has poles at the zeroes of $\Delta(\lambda)$. Actually the equation $\Delta(\lambda) = 0$ is the mode equation (2.88) provided we replace u, u_1, u_2 and λ by $(-jh)$, $(-jh_1)$, $(-jh_2)$ and $(-j\Gamma)$, respectively. It is easy to see that the roots occur by opposite pairs $\pm \lambda^{(0)}$, $\pm \lambda^{(1)}$, ... where, by convention, $-\pi < \arg \lambda^{(i)} \leq 0$.

Up to now the integral (2.107) is calculated along the C-contour. The behaviour of $H_o^{(2)}(\lambda\rho)$ and $F(\lambda)$ is such that this contour may be completed by portions of circles of infinite radius located in the lower half plane. The contour may further be transformed into C_1 shown on Figure 2.6, provided we extract the contributions of the residues at the poles $\lambda^{(0)} = -j\Gamma^{(0)}$, $\lambda^{(1)} = -j\Gamma^{(1)}$... The integral along the remaining contour C_1 gives the unguided radiation, while the pole contribution yields the guided modes. Keeping only the latter, we may write

$$\pi_z = \pi M \sum_{n=0}^{\infty} \frac{H_o^{(2)}(\lambda\rho)\, F(\lambda)\lambda}{h \frac{d\Delta}{d\lambda}} \qquad (2.108)$$

After some manipulation and replacing $\lambda^{(n)}$ by $-j\Gamma^{(n)}$, we obtain

$$\pi_z = \frac{M}{a} \sum_{n=0}^{\infty} \frac{\Lambda}{R_2} K_o(\Gamma\rho)\, f(z)\, f(z_o) \qquad (2.110)$$

where

$$f(z) = e^{jhz} + R_2\, e^{-jhz} \qquad (2.111)$$

$$\Lambda = \left[1 - j \frac{h}{2\lambda a R_1 R_2} \frac{\partial(R_1 R_2)}{\partial\lambda}\right]^{-1} \qquad (2.112)$$

The various terms of the expansion, including the factor Λ, need of course to be evaluated at $\lambda = \lambda^{(n)}$. The main components of the fields follow from Appendix B formulas and are given by

$$E_z = \frac{M}{a} \sum_{n=0}^{\infty} \frac{\Lambda \Gamma^2}{R_2} K_o(\Gamma\rho)\, f(z)\, f(z_o) \qquad (2.113)$$

$$H = \frac{-j\omega\varepsilon M}{a} \sum_{n=0}^{\infty} \frac{\Lambda\Gamma}{R_2} K_1(\Gamma\rho)\, f(z)\, f(z_o) \qquad (2.114)$$

In the limit $|\Gamma\rho| \to \infty$, we may use the approximation

$$K_n(\Gamma\rho) \approx \sqrt{\frac{\pi}{2\Gamma\rho}}\, e^{-\Gamma\rho} \qquad (2.115)$$

and retrieve cylindrical waves which are closely related to the plane waves discussed in section 2.6.1.

These formulas have important applications in several domains of electromagnetic wave propagation, namely for the excitation of waves in the earth-ionosphere waveguide, along dielectric slabs, etc. Here we are particularly interested in the propagation along a low conductivity layer like a coal seam. In this application, it may in general be assumed that the upper and lower half spaces have the same electrical parameters. The mode equation then takes the form

$$R_1 = R_2 = \pm e^{jha} \qquad (2.116)$$

where the upper and lower sign apply to the even and odd modes, respectively.

This yields

$$\frac{f(z)\, f(z_o)}{R_2} = \begin{cases} 4 \cos\left[h(z - a/2)\right] \cos\left[h(z_o - a/2)\right] \\ 4 \sin\left[h(z - a/2)\right] \sin\left[h(z_o - a/2)\right] \end{cases} \qquad (2.117)$$

respectively. Note that h is complex. Furthermore, the excitation factor takes the form (Wait, 1976a) *

$$A = \left[1 + \frac{k_1^2 - k^2}{k_1^2 - k^2 + h^2} \frac{\sin(ha)}{ha}\right]^{-1} \qquad (2.118)$$

where A has to be evaluated for the mode under consideration. An interesting limiting case already discussed in section 2.6.1 is that of perfectly conducting walls : we then have $A^{(0)} = 1/2$, $A^{(n)} = 1$ for $n \neq 0$.

2.6.3. Excitation by a horizontal magnetic dipole

Alternatively, waves with vertical polarisation can also be excited by a horizontal magnetic dipole. This type of source is realized as a loop or ferrite antenna with horizontal axis. It is obviously not omnidirectional as the electric dipole : as expected, radiation is maximum on the broadside of the dipole and zero on the axis. The radiation of the horizontal dipole can be calculated using methods similar to those of the preceding section and is available (Wait, 1952). However the problem is more complicated since two potential components are required and all the six components of the electromagnetic field are non-zero. One of the potential components is necessarily a magnetic vector parallel to the dipole. The other one may be a vertical magnetic potential or an electric potential parallel to the dipole.

A simpler approach yielding a partial answer is to use the results of the foregoing section by means of the reciprocity theorem. The form of the theorem which will be used here is as follows. Consider two experiments carried out in a non necessarily homogeneous but isotropic medium. In the first experiment, electric and magnetic current densities $\overline{J}'_a$, $\overline{J}'_{ma}$ are applied simultaneously at finite distance and radiate fields $\overline{E}'$, $\overline{H}'$. In the second experiment, applied current densities $\overline{J}''_a$, $\overline{J}''_{ma}$ radiate fields $\overline{E}''$, $\overline{H}''$. Then we have

$$\int (\overline{J}'_a \cdot \overline{E}'' - \overline{J}'_{ma} \cdot \overline{H}'')\, dV = \int (\overline{J}''_a \cdot \overline{E}' - \overline{J}''_{ma} \cdot \overline{H}')\, dV \qquad (2.119)$$

where the volume integrals are over whole space.

In the present application, we consider for the first experiment a vertical electric dipole located at the point of vector position $\overline{r}' = (\rho', \phi', z')$

$$\overline{J}'_a = I\, ds\, \delta(\overline{r} - \overline{r}')\, \overline{u}_z \qquad (2.120)$$

and no magnetic current. The fields $(\overline{E}', \overline{H}')$ of this dipole were calculated in section 2.6.2. In particular, as results from (2.90) and (2.114), we have

$$\overline{H}'(0, \phi, z_o) = \frac{-I\, ds}{4\pi a} \sum_{n=0}^{\infty} \frac{A\Gamma}{R_2} K_1(\Gamma\rho')\, f(z')\, f(z_o)\, \overline{u}_\phi \qquad (2.121)$$

when we keep only the guided modes.

In the second experiment, the source is a magnetic dipole located at a height z_o on the z-axis and parallel to the x-axis

$$\overline{J}''_{ma} = I_m\, ds\, \delta(\overline{r})\, \overline{u}_x \qquad (2.122)$$

The fields $(\overline{E}'', \overline{H}'')$ of this source are the unknowns of the problem.

Using the reciprocity theorem, we obtain the vertical electric field radiated by this magnetic dipole at the point (ρ', ϕ', z')

$$E''_z(\rho', \phi', z') = \frac{-I_m\, ds \cos\phi'}{4\pi a} \sum_{n=0}^{\infty} \frac{A\Gamma}{R_2} K_1(\Gamma\rho')\, f(z')\, f(z_o) \qquad (2.123)$$

The other field components cannot all be directly obtained from E''_z. However at some distance from the magnetic dipole, the main field components are E''_z and H''_ϕ, with the relation

$$H''_\phi = \frac{-j\omega\varepsilon}{\Gamma} E''_z \qquad (2.124)$$

In using (2.123) we have to remember that an infinitesimal loop is equivalent to a magnetic dipole as given by eq. (2.5).

* In equation (3) of this paper the factor $(kh)^{-1}$ should be replaced by $(2kh)^{-1}$.

2.7. NATURAL PROPAGATION IN EMPTY TUNNELS

2.7.1. Introduction : planar air waveguide

Natural propagation of electromagnetic waves in empty tunnels was explained qualitatively in section 1.2.1, where reference was made to attenuation formulas valid for waveguides with highly conducting walls. This approach is undoubtedly invalid in the VHF and UHF bands for tunnel walls made of rock, concrete, bricks and similar materials. Indeed, the frequency is then well above the transition frequency of these materials (i.e. $\omega\varepsilon >> \sigma$), which consequently behave as lossy dielectrics rather than conductors. It is felt that a more refined analysis is required.

To start with this problem, we consider the simplest geometry consisting of a planar air slab located between two conducting half-spaces having the same electrical characteristics. Mathematically this problem is identical with the one solved in section 2.6. However we are interested here in the case where the slab thickness is several times the wavelength in air, and at frequencies such that the complex dielectric constant of the surrounding medium, denoted by

$$\kappa_1' = \kappa_1 + \frac{\sigma_1}{j\omega\varepsilon_0} \tag{2.125}$$

is close to κ_1. We will assume that the latter takes on a value which is neither close to unity nor large.

The question we want to answer is : can we have modes with propagation constant close to that of plane waves in air, i.e. such that $\Gamma \approx jk_0$? For this purpose, we rewrite the mode equation (2.88) as

$$e^{2ua} = R^2 \tag{2.126}$$

with the reflection coefficient R given by

$$R = \frac{\kappa_1 ua - u_1 a}{\kappa_1' ua + u_1 a} \tag{2.127}$$

where

$$ua = \sqrt{-(k_0 a)^2 - (\Gamma a)^2} \tag{2.128}$$

$$u_1 a = \sqrt{(k_0 a)^2 (\kappa_1' - 1) + (ua)^2} \tag{2.129}$$

The assumption $\Gamma \approx jk_0$ is equivalent to $|ua| << k_0 a$. As κ_1' takes on a moderate

value, this entails $|ua| << |u_1 a|$ and $|\kappa_1' ua| << |u_1 a|$. We may write

$$R = -\frac{1 - \xi}{1 + \xi} \tag{2.130}$$

where

$$\xi = \frac{\kappa_1' ua}{u_1 a} \tag{2.131}$$

and $|\xi| << 1$. It is seen that the reflection factor is close to (-1). Consequently, the mode equation (2.126) can be satisfied if

$$ua = p\pi j + \nu \tag{2.132}$$

where $|\nu| << 1$. Using the first two terms of a Taylor series for the both sides of the mode equation, we obtain

$$ua = \frac{p\pi j}{1 + \dfrac{2\kappa_1'}{jk_0 a \sqrt{\kappa_1 - 1}}} \quad ; \quad p > 0 \tag{2.133}$$

where the determination $-\frac{\pi}{2} < \arg u_1 \leq \frac{\pi}{2}$ was taken into account. The value $p = 0$ has to be discarded since it violates this condition.

It can be seen from this equation that for $p \neq 0$, the condition $|ua| << k_0 a$ can only be met *if* $k_0 a >> 1$ *and only for those modes for which* $p\pi << k_0 a$. The propagation constant of these modes can now be obtained from (2.128) and (2.133). Taking into account that $\kappa_1' \approx \kappa_1$ and separating into real and imaginary parts, we obtain

$$\beta_n^{(v)} \approx \sqrt{k_0^2 - (n+1)^2 \frac{\pi^2}{a^2}} \tag{2.134}$$

$$\alpha_n^{(v)} \approx \frac{2(n+1)^2 \pi^2}{k_0^2 a^3} \operatorname{Re} \frac{\kappa_1'}{\sqrt{\kappa_1' - 1}} \tag{2.135}$$

where $n = p - 1$ rather than p is the mode order (this choice is made to establish a one-to-one correspondence with the classical numbering of modes in metallic waveguides). The subscript v has been added to α and β to recall that we are studying modes with the main polarisation vertical. Equation (2.134) is identical

with that of a planar waveguide with perfectly conducting walls. Eq. (2.135) for the specific attenuation is quite remarkable. It shows that the attenuation is proportional to the square of (n + 1) and inversely proportional to the square of frequency and to the third power of the slab thickness. Furthermore it is determined by the dielectric constant κ_1 of the external medium rather than by its electric conductivity.

These results have a simple physical meaning. The modes consist of a plane wave which bounces against the upper and lower half-spaces. The complex incidence angle is given by $\sin\theta = \Gamma/(jk)$ and is close to $\pi/2$. It is know that $R \approx -1$ at grazing incidence. The attenuation is due to the slight departure from total reflection. The small amount of power which is refracted into the wall is the cause of attenuation; under the condition $\omega\varepsilon_o \kappa_1 >> \sigma_1$, it is governed by κ_1 rather than by σ_1. The main effect of the wall conductivity is to cause a rapid attenuation of the refracted wave into the external media. This role is nevertheless essential in the propagation mechanism. Indeed, if the external media were lossless dielectrics, the refracted wave would not be attenuated and guided modes would not exist since an infinite power would be required.

Up to now, the attention was focused on the modes with the main polarisation vertical but the frequency range of interest in this section is such that the modes with horizontal polarisation are also above cutoff. It is easy to show that the relevant mode equation is now

$$e^{2ua} = S^2 \tag{2.136}$$

where

$$S = \frac{u - u_1}{u + u_1} \tag{2.137}$$

is the reflection factor for waves with the electric field perpendicular to the plane of incidence. It is easy to repeat the foregoing discussion for these modes. This yields

$$\beta_n^{(h} \approx \sqrt{k_o^2 - \left(n\frac{\pi}{a}\right)^2} \tag{2.138}$$

$$\alpha_n^{(h} \approx \frac{2(n\pi)^2}{k^2 a^3}\ \mathrm{Re}\ \frac{1}{\sqrt{\kappa_1' - 1}} \tag{2.139}$$

Note that $n > 0$ is the mode order.

2.7.2. Geometrical optical approach for the planar air waveguide

Radiation of a dipole located inside the planar air waveguide may be calculated by the method outlined in section 2.6.2. The foregoing interpretation of the guided modes in terms of reflections on the guide wall suggests that the problem could also be solved by summing the contributions of rays undergoing reflections on the guide walls. This geometrical optical approach has been developped by Mahmoud and Wait (1974c).

We will only sketch the method by which a ray model can be deduced from the rigorous solution given by eq. (2.107) for a vertical electric dipole, assuming that the top and bottom media are identical. the inverse denominator of the integrand possesses the Taylor series expansion

$$\Delta^{-1} = \frac{1}{e^{jha}(1 + Re^{-2jha})}$$

$$= e^{-jha} \sum_{n=0}^{\infty} (-1)^n R^{2n} e^{-2jhna} \tag{2.140}$$

Inserting this series into eq. (2.107) and evaluating the integral of each term by the method of the stationary phase (Morse and Fesbach, 1953) provides a result that can be interpreted as a sum of rays emanating from a double infinity of images or alternatively having undergone multiple reflections on the top and bottom boundaries. Figure 2.7 illustrates the process.

This method however is not very accurate unless the phase variation of R^{2n} with h is duly taken into account. It has the advantage of giving a physical interpretation to complex mathematical expressions.

2.7.3. Rectangular tunnel

The geometrical parameters of a rectangular tunnel are shown on Figure 2.8. An attempt to solve this problem exactly leads to an extremely high complexity. Indeed, if we use Cartesian coordinates, it is required to write different analytical expressions for two potentials inside the waveguide and in each of the eight external regions. Boundary conditions must then be expressed at each of the twelve interfaces. Alternatively, if Fourier transforms are used in the analysis, for instance on the x coordinate, one has to match Fourier transforms on the domains

$x < 0$, $0 < x < a$ and $x > a$. This brings to a complex three-part Wiener-Hopf problem with two coupled functions corresponding to the potentials used. Simplifying assumptions or approximate methods are obviously required.

a) Perfectly conducting side walls

A first simplifying assumption is to consider perfectly conducting side walls. In this case, we assume that regions $x < 0$ and $x > a$, $-\infty < y < \infty$, are perfectly conducting. We are now left with only three regions in which different analytical expressions must be used. This model may be a good one for a tunnel bored in a coal seam embedded in highly conducting rock. We will assume that the media for $0 < x < a$ and either $y < 0$ or $y > b$ have a dielectric constant κ_1, a conductivity σ_1 and a complex wavenumber $k_1 = k_o \sqrt{\kappa_1'}$ where $\kappa_1' = \kappa_1 + \sigma_1/(j\omega\varepsilon_o)$ is the complex dielectric constant.

A complete analysis of the radiation of a vertical or horizontal electric dipole located at a point of coordinates $(x_o, y_o, 0)$ inside the tunnel is available in the literature (Mahmoud and Wait, 1974c). A complete presentation of this theory would be beyond the scope of the present course. We will only discuss some points and give the final results.

The fundamental theorem on potentials given in section 2.2 suggests that the problem should be solved using two scalar potentials π'_x and π''_x. It however appears that expressing the boundary conditions at the interfaces is made easier when π'_y and π''_y are used, since they do not couple in the boundary conditions.

The analysis has many points in common with the one performed in section 2.6.2 for a horizontally stratified medium. The vertical walls impose that the solution contains terms of the type $\cos(m\pi x/a)$ and $\sin(m\pi x/a)$, where m is an integer. Instead of eq. (2.79) the vertical propagation constants are now defined by

$$u_m = \left[-k_o^2 + (m\pi/a)^2 + h^2\right]^{1/2} \tag{2.142}$$

$$u_{m1} = \left[-k_1^2 + (m\pi/a)^2 + h^2\right]^{1/2} \tag{2.143}$$

Instead of the mode equations (2.128) - (2.137) and (2.138) - (2.137), one now finds

$$\Delta_m^{(v)} = 1 - R_m^2 \, e^{-2u_m b} = 0 \tag{2.144}$$

$$R_m = \frac{k_1^2 u_m - k_o^2 u_{m1}}{k_1^2 u_m + k_o^2 u_{m1}} \tag{2.145}$$

and

$$\Delta_m^{(h)} = 1 - S_m^2 \, e^{-2u_m b} = 0 \tag{2.146}$$

$$S_m = \frac{u_m - u_{m1}}{u_m + u_{m1}} \tag{2.147}$$

respectively.

The equation $\Delta_m^{(h)} = 0$ corresponds to a pole of π''_y. As results from eq. (A.25) of Appendix A, modes derived from this single potential component have $E_y = 0$. The transverse electric field is therefore horizontal and these modes are labelled $E_{mn}^{(h)}$ to recall this. It will be understood that n indicates the n-th root of eq. (2.146). Similarly (2.144) results from poles of π'_y. They have $H_y = 0$ and should be labelled $H_{mn}^{(h)}$ but we prefer to call them $E_{mn}^{(v)}$ because they are characterized by $|E_y| >> |E_x|$ in large tunnels. They are mainly vertically polarized.

Finally, like we did in section 2.7.1 for the planar air waveguide, it is possible to establish approximations valid when the tunnel cross-section is much larger than the wavelength. For $E_{mn}^{(h)}$ modes, we find

$$\beta_{mn}^{(h)} \approx \sqrt{k_o^2 - \left(\frac{m\pi}{a}\right)^2 - \left(\frac{n\pi}{b}\right)^2} \tag{2.148}$$

$$\alpha_{mn}^{(h)} \approx \frac{2(n\pi)^2}{k_o^2 \, b^3} \, \mathrm{Re} \, \frac{1}{\sqrt{\kappa_1' - 1}} \tag{2.149}$$

with $m \geq 0$, $n > 0$, whereas for $E_{mn}^{(v)}$ modes,

$$\beta_{mn}^{(v)} \approx \sqrt{k_o^2 - \left(\frac{m\pi}{a}\right)^2 - \frac{(n+1)^2 \pi^2}{b^2}} \tag{2.150}$$

$$\alpha_{mn}^{(v)} \approx \frac{2(n+1)^2 \pi^2}{k_o^2 \, b^3} \, \mathrm{Re} \, \frac{\kappa_1'}{\sqrt{\kappa_1' - 1}} \tag{2.151}$$

From the present analysis it results that a vertical electric dipole excites only $E_{mn}^{(v)}$ modes. A horizontal electric dipole excites mainly $E_{mn}^{(h)}$ modes but also, with a smaller amplitude, $E_{mn}^{(v)}$ modes. Common to both types of modes is the fact that

the specific attenuation is independent on m wall above the cutoff frequency. The specific attenuation of $E_{mn}^{(h)}$ modes may be significantly smaller than that of $E_{mn}^{(v)}$ modes, particularly when the dielectric constant κ_1 is high. Finally, it should be observed that the condition $(k_o\ a)^2 >> (m^2 + n^2)\pi^2$ or $(k_o a)^2 >> [m^2 + (n+1)^2]\pi^2$ entails that the fields of these modes are approximately TEM.

b) Approximations for the tunnel with four imperfectly conducting walls

It has been explained that an exact analytical approach to this problem would lead to an extreme complexity. Several approximate methods for calculating the mode propagation constants of this structure have been published and will be discussed.

The analysis of Emslie et al. (1975) is restricted to the lowest-order $E^{(v)}$ and $E^{(h)}$ modes, but it can easily be extended to higher-order modes. As the structure is symmetrical we will restrict our attention to the $E^{(h)}$ mode. These authors assume that the fields inside the waveguide may be written in the form

$$E_x = E_o \cos\left[k_1(x - a/2)\right] \cos\left[k_2(y - b/2)\right] \exp(-jk_3 z)$$

$$E_y = 0$$

$$E_z = (jk_1/k_3)\, E_o \sin\left[k_1(x - a/2)\right] \cos\left[k_2(y - b/2)\right] \exp(-jk_3 z)$$

$$H_x = k_1 k_2/(\omega\mu_o\, k_3)\, E_o \sin\left[k_1(x - a/2)\right] \sin\left[k_2(y - b/2)\right] \exp(-jk_3 z)$$

$$H_y = (k_1^2 + k_3^2)/(\omega\mu_o\, k_3)\, E_o \cos\left[k_1(x - a/2)\right] \cos\left[k_2(y - b/2)\right] \exp(-jk_3 z)$$

$$H_z = jk_2/(\omega\mu_o)\, E_o \cos\left[k_1(x - a/2)\right] \sin\left[k_2(y - b/2)\right] \exp(-jk_3 z) \qquad (2.152)$$

where the coordinate wave numbers k_1, k_2, k_3 may be complex and must satisfy the relation $k_1^2 + k_2^2 + k_3^2 = k_o^2$. Actually this is the type of expression which can be obtained by separation of variables with a single scalar magnetic potential π''_y. The reader will remember that this type of solution was obtained for the $E^{(h)}_y$ modes of the tunnel with perfectly conducting side walls. Similar expressions are written, with adequate notations, for the Regions A_{-o}, A_{+o}, A_{o+} and A_{o-} of Figure 2.8. It then appears that the boundary conditions cannot be exactly satisfied. When the tunnel cross-section is large, approximations similar to those used in previous sections can be made and the boundary conditions can be exactly satisfied for all field components on the horizontal walls and for E_z, H_y on the vertical walls, but not for the axial component H_z. It is however observed that this component is much smaller than H_y and consequently the boundary conditions are aproximately satisfied.

A very similar approach was used by Laakman and Steier (1976). These authors however start with more general field expressions which are derived from two scalar potential components. All the six components of the fields are now non-zero. Here also, it appears that the boundary conditions can be satisfied only in an approximate way. Actually, this analysis is equivalent to that of Emslie et al. since the part of the solution which can be obtained from a π'_y potential (assumed to be zero by Emslie) is of second-order magnitude. It is thus not surprising that the approximate results obtained in the two papers are identical.

Common to thses analyses, is the fact that the fields in the corner regions A_{--}, A_{-+}, A_{+-} and A_{++} of Figure 2.8 do not intervene in the derivation of the solution, which therefore neglects the effect of the corners. Actually, the solution does not take the corner regions into account and the latter may even contain a non-homogeneous medium. The authors were consequently allowed to assume that the electrical parameters of top and bottom walls differed from those of the vertical walls.

Assuming that the horizontal and vertical walls have complex dielectric constants κ'_h and κ'_v, respectively, the propagation constant of the $E_{mn}^{(v)}$ mode is given approximately by

$$\Gamma_{mn}^{(v)} = \alpha_{mn}^{(v)} + j\,\beta_{mn}^{(v)} \qquad (2.153)$$

$$\alpha_{mn}^{(v)} = \frac{2(m+1)^2\pi^2}{k_o^2\, b^3}\ \mathrm{Re}\ \frac{\kappa'_h}{\sqrt{\kappa'_h - 1}} + \frac{2(n+1)^2\pi^2}{k_o^2\, a^3}\ \mathrm{Re}\ \frac{1}{\sqrt{\kappa'_v - 1}} \qquad (2.154)$$

$$\beta_{mn}^{(v)} = \sqrt{k_o^2 - \left[\frac{(m+1)\pi}{a}\right]^2 - \left[\frac{(n+1)\pi}{b}\right]^2} \qquad (2.155)$$

where the mode indices m, n run from zero to infinity. The main components of the transverse field for this mode are given by

$$E_y = \sin \frac{(m+1)\pi x}{a} \sin \frac{(n+1)\pi y}{b} \exp(-\Gamma_{mn}^{(v)} z) \qquad (2.156)$$

$$H_x = \sqrt{\frac{\mu_o}{\epsilon_o}} E_y \qquad (2.157)$$

The results for the $E_{mn}^{(h)}$ mode are obtained by interchanging the x and y axes. These approximations are valid under the assumptions

$$k_o a \ , \ k_o b >> 1$$

$$|\kappa_v' - 1| >> \frac{(m+1)\pi}{k_o a} \qquad (2.158)$$

$$\left|\frac{\kappa_h'}{\kappa_h' - 1}\right| >> \frac{(n+1)\pi}{k_o b}$$

These results are remarkable in several respects. The specific attenuation of the $E_{mn}^{(v)}$ mode is obtained by adding the values of α for waveguides with perfectly conducting horizontal walls and with perfectly conducting vertical walls, keeping the other walls unchanged. The main transverse field components are approximately zero on all the four walls.

Another but still very similar approach to the problem of the rectangular waveguide with four imperfectly conducting walls was given by Andersen et al. (1975). These authors assume that the field inside the waveguide is composed of four plane waves with vectorial wavenumbers (k_x, k_y, k_z), $(-k_x, k_y, k_z)$, $(k_x, -k_y, k_z)$ and $(-k_x, -k_y, k_z)$ and express that these waves are related by plane wave reflection coefficients on the waveguide walls : for instance, the first wave is reflected into the second one at the interface x = a. It can be shown that this formulation does not differ in any way from Laakman and Steier's (1978). These methods implicitely contain the proof that the guided modes of the rectangular structure cannot be found by separation of the variables x and y. Some superiority of Andersen et al.'s analysis may be claimed from the fact that they use a r.m.s. minimisation algorithm to find an approximate solution of the overdetermined set of boundary conditions, rather than ignoring some of these.

It is also possible, at least when the complex dielectric constant of the side walls is relatively large, to obtain a good approximation by replacing the boundary conditions on all walls by a surface impedance condition (Wait, 1980).

Finally it must be mentioned that the geometrical approach developed by Mahmoud and Wait (1974c) and analyzed in section 2.7.2 for the planar air waveguide has been extended by these authors to the waveguide with four imperfectly conducting walls. This method suffers from the weakness mentioned earlier but no alternative way of solving excitation problems has been proposed yet.

2.7.4. Circular tunnel

The geometry of the circular tunnel (Figure 2.9) lends itself much easier to exact analytical solution of Maxwell's equations than the rectangular tunnel. Formally the problem we are involved in is identical to that of the dielectric waveguide (Stratton, 1941) which has taken a fundamental importance with fiber optics, but we are here interested in the guided modes of this structure for a quite different range of parameters. The inside of the waveguide, of radius a, is filled with air. The external medium has a complex dielectric constant κ_1', a permeability μ_1 and a complex wavenumber k_1. We will use solutions of Maxwell's equations in the form (B.25-33) of Appendix B and denote

$$\Lambda = \sqrt{k_o + \Gamma^2} \quad ; \quad -\pi < \arg \Lambda \leq 0 \qquad (2.159)$$

$$\Lambda_1 = \sqrt{k_1 + \Gamma^2} \quad ; \quad -\pi < \arg \Lambda_1 \leq 0 \qquad (2.160)$$

The solutions which remain finite on the tunnel axis and tend toward zero to infinity are the form

$$E_\rho = \sum_{m=o}^{\infty} \left[-\frac{j\omega\mu_o m}{\rho} P_m J_m(\Lambda\rho) - \Lambda\Gamma Q_m J_m'(\Lambda\rho) \right] \cos\left[m(\phi - \phi_m)\right] \qquad (2.161)$$

$$E_\phi = \sum_{m=o}^{\infty} \left[j\omega\mu_o \Lambda P_m J_m'(\Lambda\rho) + \frac{\Gamma m}{\rho} Q_m J_m(\Lambda\rho) \right] \sin\left[m(\phi - \phi_m)\right] \qquad (2.162)$$

$$E_z = \sum_{m=o}^{\infty} \Lambda^2 Q_m J_m(\Lambda\rho) \cos\left[m(\phi - \phi_m)\right] \qquad (2.163)$$

$$H_\rho = \sum_{m=0}^{\infty} \left[-\Lambda\Gamma P_m J_m'(\Lambda\rho) - \frac{j\omega\varepsilon_0 m}{\rho} Q_m J_m(\Lambda\rho) \right] \sin\left[m(\phi - \phi_m)\right] \qquad (2.164)$$

$$H_\phi = \sum_{m=0}^{\infty} \left[-\frac{\Gamma m}{\rho} P_m J_m(\Lambda\rho) - j\omega\varepsilon_0 \Lambda Q_m J_m'(\lambda\rho) \right] \cos\left[m(\phi - \phi_m)\right] \qquad (2.165)$$

$$H_z = \sum_{m=0}^{\infty} \Lambda^2 P_m J_m(\Lambda\rho) \sin\left[m(\phi - \phi_m)\right] \qquad (2.166)$$

where the angles ϕ_m are arbitrary, for the inside of the tunnel. In the external medium the arbitrary constants P_m, Q_m should be replaced by A_{m1}, B_{m1}, ε_0, μ_0, Λ by ε_1, μ_1, Λ_1; and $J_m(\Lambda\rho)$ by $H_m^{(2)}(\Lambda_1\rho)$. The mode equation is obtained by expressing the continuity of the tangential field at $\rho = a$ and writing that the determinant of the system of equations obtained this way is zero. This yields the classical equation

$$\left[\frac{J_m'(\Lambda a)}{\Lambda a\, J_m(\Lambda a)} - \frac{\mu_1}{\mu_0} \frac{H_m^{(2)'}(\Lambda_1 a)}{\Lambda_1 a\, H_m^{(2)}(\Lambda_1 a)}\right]\left[\frac{J_m'(\Lambda a)}{\Lambda a\, J_m(\Lambda a)} - \kappa_1' \frac{H_m^{(2)'}(\Lambda_1 a)}{\Lambda_1 a\, H_m^{(2)}(\Lambda_1 a)}\right]$$

$$= -\left(\frac{m\Gamma}{k_0}\right)^2 \left[\frac{1}{(\Lambda a)^2} - \frac{1}{(\Lambda_1 a)^2}\right]^2 \qquad (2.167)$$

For the remainder of this section we will assume that $\mu_1 = \mu_0$.

This equation can of course be solved numerically. Here we are interested in developing approximations valid when the tunnel cross-section is large compared with the wavelength. This is the kind of work which was performed in section 2.7.1 for the planar waveguide. Actually we follow the analysis made by Marcatili and Schmeltzer (1964) in the context of optical transmission, but we will differ in the mode nomenclature. We are examining the following question : assuming that $k_0 a \gg 1$ can we have modes with a propagation constant Γ close to (jk_0), i.e. such that $|\Lambda a| \ll k_0 a$? Again, provided $|\kappa_1'|$ is neither close to nor large compared with unity, this entails $|\Lambda a| \ll |\Lambda_1 a|$, $|\Lambda_1 a| \gg 1$. Now, for those modes for which $|\Lambda_1 a| \gg m$, we may use the large argument approximations of the Hankel function and of its derivative. This yields

$$\frac{H_m^{(2)'}(\Lambda_1 a)}{H_m^{(2)}(\Lambda_1 a)} \simeq -j \qquad \text{if } |\Lambda_1 a| \gg m \qquad (2.168)$$

This right-hand side of (2.167) may be approximated by $(m/\Lambda^2 a^2)^2$. Consequently this equation reduces to the approximate form

$$\left[\frac{J_m'(\Lambda a)}{J_m(\Lambda a)} + j\frac{\Lambda a}{\Lambda_1 a}\right]\left[\frac{J_m'(\Lambda a)}{J_m(\Lambda a)} + j\kappa_1' \frac{\Lambda a}{\Lambda_1 a}\right] \simeq \frac{m^2}{(\Lambda a)^2} \qquad (2.169)$$

We will discuss separately the cases $m = 0$ and $m \neq 0$. Indeed for $m = 0$ the right-hand side of (2.167) is zero and this equation is split into two independent ones, the solutions of which yield TE and TM modes. The parts of the [illegible] due to the electric and magnetic potentials are indeed uncoupled in [illegible]. The results of the discussion are summarized below. We denote by ξ_{pq} the q th non zero root of $J_p(\xi) = 0$ with $p > 0$.

Case a : $m = 0$, TE_{0n} modes

The mode equation

$$\frac{J_0'(\Lambda a)}{\Lambda a\, J_0(\Lambda a)} - \frac{H_0^{(2)'}(\Lambda_1 a)}{\Lambda_1 a H_0^{(2)}(\Lambda_1 a)} = 0 \qquad (2.170)$$

or, in approximate form

$$\frac{J_0'(\Lambda a)}{J_0(\Lambda a)} + j\frac{\Lambda a}{\Lambda_1 a} \simeq 0 \qquad (2.171)$$

expresses the continuity of $E_{\phi 0}$ and H_{z0} and yields the TE modes :

$$E_{\phi 0} = j\omega\mu_0 \Lambda P_0 J_0'(\Lambda\rho) \qquad (2.172)$$

$$H_{\rho 0} = -\Gamma \Lambda P_0 J_0'(\Lambda\rho) \qquad (2.173)$$

$$H_{z0} = \Lambda^2 P_0 J_0(\Lambda\rho) \qquad (2.174)$$

where we may use the identity $J_0'(\Lambda\rho) = -J_1(\Lambda\rho)$. The mode equations has the ap-

proximate solution

$$A_{on}a = \xi_{1n}\left[1 + j\frac{1}{k_o a\sqrt{\kappa_1' - 1}}\right] \tag{2.175}$$

and the attenuation constant is approximately

$$\alpha_{on} = \frac{\xi_{1n}^2}{k_o^2 a^3}\ \mathrm{Re}\frac{1}{\sqrt{\kappa' - 1}} \tag{2.176}$$

Case b : m = 0, TM_{on} modes

The mode equation

$$\frac{J_o'(Aa)}{Aa\,J_o(Aa)} - \kappa_1'\frac{H_o^{(2)'}(A_1 a)}{A_1 a H_o^{(2)}(A_1 a)} = 0 \tag{2.177}$$

or, in approximate form

$$\frac{J_o'(Aa)}{J_o(Aa)} + j\kappa_1'\frac{Aa}{A_1 a} = 0 \tag{2.178}$$

expresses the continuity of E_{zo} and $H_{\phi o}$ and yields the TM modes :

$$E_{\rho o} = -\Gamma A Q_o J_o'(A\rho) \tag{2.179}$$

$$E_{zo} = A^2 Q_o J_o(A\rho) \tag{2.180}$$

$$H_{\phi o} = -j\omega\varepsilon_o A Q_o J_o'(A\rho) \tag{2.181}$$

The mode equation yields the approximate solutions

$$A_{on}a = \xi_{1n}\left[1 + j\frac{\kappa_1'}{k_o a\sqrt{\kappa_1' - 1}}\right] \tag{2.182}$$

and

$$\alpha_{on} = \frac{\xi_{1n}^2}{k_o^2 a^3}\ \mathrm{Re}\frac{\kappa_1'}{\sqrt{\kappa_1' - 1}} \tag{2.183}$$

Case c : m ≠ 0, hybrid $EH_{mn}^{\pm}$ modes

The study of solutions of the complete mode equation in the approximate form (2.189) yields solutions

$$A_{mn}^{\pm} = \xi_{m\pm1,n}\left[1 + k\frac{\kappa_1' + 1}{2k_o a\sqrt{\kappa_1' - 1}}\right] \tag{2.184}$$

and

$$\alpha_{mn}^{\pm} = \frac{\xi_{m\pm1,n}^2}{k_o^2 a^3}\ \mathrm{Re}\frac{\kappa_1' + 1}{2\sqrt{\kappa_1' - 1}} \tag{2.185}$$

whereas the electromagnetic fields are nearly TEM and approximately given by

$$E_{\rho m}^{\pm} = J_{m\pm1}(\xi_{m\pm1,n}\,\rho/a)\cos\left[m(\phi - \phi_m)\right] \tag{2.186}$$

$$E_{\phi m}^{\pm} = \pm J_{m\pm1}(\xi_{m\pm1,n}\,\rho/a)\sin\left[m(\phi - \phi_m)\right] \tag{2.187}$$

$$\bar{H}_t = \frac{k_o}{\omega\mu_o}\bar{u}_z \times \bar{E}_t \tag{2.188}$$

where we have neglected a common amplitude factor. We recall that ϕ_m is arbitrary and represents the azimuthal degeneracy of the structure.

Taking into account the values $\xi_{01} = 2.405$ and $\xi_{11} = 3.832$, it is seen that, for κ_1 real, the mode with the lowest attenuation is TE_{01} if $\kappa_1 < 4.08$ and EH_{11}^{-} if $\kappa_1 > 4.08$. It is interesting to collect the conditions under which these approximate results are valid; in practical form :

$$k_o a \gg 1$$

$$\left|k_o a\sqrt{\kappa_1' - 1}\right| \gg m \pm 1 \tag{2.189}$$

$$\left|k_o a\sqrt{\kappa_1' - 1}\right| \gg \frac{\xi_{m\pm1,n}^2}{m}\left|\sqrt{\kappa_1'}\right| \qquad \text{if } m \neq 0$$

2.7.5. Some general conclusions

Although the exact solution of the mode equation for the various shapes of tunnels can only be obtained numerically, it is clear that a cutoff effect exists as for waveguides with highly conducting walls. The model of the latter may be used for approximate predictions of the cutoff frequency. It however completely fails to predict the attenuation above this frequency, i.e. in the useable frequency range.

Quite generally, for metallic waveguides above the cutoff, the specific attenuation increases with frequency. In tunnels on the contrary, all formulas that have been established, namely (2.135, 139, 149, 151, 154, 176, 183 and 185), show that the attenuation decreases as the square of frequency. Another characteristic is that it is inversely proportional to the cube of the tunnel size. The fields of the guided modes are only approximately TEM. All these properties explain very well experimental data like those of Figure 1.3 and 1.4.

One should tend to conclude that the highest frequencies are the best suited for natural propagation in tunnels. This is only true for unobstructed straight tunnels with smooth walls. Very few studies of propagation in curved tunnels have been made (Mahmoud and Wait, 1974b; Marcatili and Schmeltzer, 1964) and the conditions under which their results are valid are rarely encountered in practice. They nevertheless have the merit of showing that the highest frequencies are not the most adequate for curved tunnels. In this case the use of wave guiding wires and cables is practically needed. We will now start the study of this problem.

2.8. GUIDED MODES OF WIRES AND LEAKY FEEDERS IN A CIRCULAR TUNNEL

2.8.1. Basic theory of guided modes

In this section, we are concerned with establishing the mode equation for the propagation of electromagnetic waves along cables parallel to the axis of a circular tunnel. By cable we mean either a conducting wire or a leaky coaxial cable. These devices may in addition be covered by a dielectric jacket and, additionaly, by a lossy layer which may be representative of dust or mud accumulated on the external surface of the cable. That a unified treatment can be used for these various devices is the result of the thin-cable approximation which has been developed in section 2.3. Let us recall that this approximation consists of modelling the cable by equation (2.19) relating the rotational symmetric part of the electric field on the external surface of the cable to the total current carried by the latter. The specific external impedance of a bare wire was obtained in section 2.4 and that of a leaky coaxial cable in section 2.5.2, where the technique for taking into account successive cylindrical layers has also been developed.

We start our analysis by considering a circular tunnel containing a single axial cable (Figure 2.9). The tunnel radius is a and the external medium has electrical permittivity ϵ_1, dielectric constant $\kappa_1 = \epsilon_1/\epsilon_0$, conductivity σ_1, complex dielectric constant $\kappa_1' = \kappa_1 - j\sigma_1/(\omega\epsilon_0)$, permeability μ_1 (which may differ from μ_0) and complex wavenumber k_1. The cable has a radius c and is located at the point (ρ_0, ϕ_0) of a system of cylindrical coordinates (ρ,ϕ,z). We are interested in finding modes with a propagation factor $\exp(-\Gamma z)$, where Γ has to be determined. The cable carries a total current $I \exp(j\omega t - \Gamma z)$. Hence the factor $\exp(j\omega t - \Gamma z)$ will be ignored in all expression of fields and potentials. We follow the method developed by Wait and Hill (1974a). Some of the basic features of this method are also present in the paper by Fontaine et al. (1974) and had previously been developed by one of these authors in his doctorate's thesis.

The primary fields excited by the cable current I, i.e. the fields which would exist if the cable were drawn into free space, may be derived from an axial electric-type Hertz potential

$$U^{(p)} = (2\pi j\omega\epsilon_0)^{-1} I K_0(v\rho_d) \qquad (2.190)$$

where

$$v = \sqrt{-k_0^2 - \Gamma^2} \quad ; \quad \frac{\pi}{2} < \arg v \leq \frac{\pi}{2} \qquad (2.191)$$

is the radial propagation constant and

$$\rho_d = \sqrt{\rho^2 + \rho_0^2 - 2\rho\rho_0 \cos(\phi - \phi_0)} \qquad (2.192)$$

is the distance from the observation point to the cable axis. The modified Hankel function may be considered as characteristic of an outgoing cylindrical wave. The addition theorem for this function

$$K_0(v\rho_d) = \sum_{m=-\infty}^{\infty} I_m(v\rho_<) K_m(v\rho_>) e^{-jm(\phi-\phi_0)} \qquad (2.193)$$

where $\rho_<$ and $\rho_>$ stand for the smallest and the largest of the radii ρ, ρ_o, provides a decomposition of this wave into a sum of outgoing waves emanating from the z-axis. This suggests seeking to solve the problem with an electric type potential U given by

$$U = (2\pi j\omega\varepsilon_o)^{-1} I \sum_{m=-\infty}^{\infty} I_m(v\rho_<) \left[K_m(v\rho_>) - R_m \frac{K_m(va)}{I_m(va)} I_m(v\rho_>)\right] \exp[-jm(\phi - \phi_o)] \quad (2.194)$$

for $\rho < a$. The added terms may be seen as incoming waves to account for the reflection by the tunnel walls. The constants R_m are to be determined and play the role of reflection factors of the tunnel wall for this type of potential. However this reflection gives also rise to fields derived from a magnetic-type Hertz potential which will be written

$$V = (2\pi j\omega\varepsilon_o)^{-1} I \sum_{m=-\infty}^{\infty} \Delta_m I_m(v\rho_<) I_m(v\rho_>) \exp[-jm(\phi - \phi_o)] \quad (2.195)$$

for $\rho < a$.

In the external medium, $\rho > a$, we use expressions containing only outgoing waves

$$U = (2\pi j\omega\varepsilon_o)^{-1} I \sum_{m=-\infty}^{\infty} F_m K_m(u\rho) \exp[-jm(\phi - \phi_o)] \quad (2.196)$$

$$V = (2\pi j\omega\varepsilon_o)^{-1} I \sum_{m=-\infty}^{\infty} G_m K_m(u\rho) \exp[-jm(\phi - \phi_o)] \quad (2.197)$$

where the radial propagation constant u is given by

$$u = \sqrt{-k_1^2 - \Gamma^2} \quad ; \quad -\frac{\pi}{2} < \arg u \leq \frac{\pi}{2} \quad (2.198)$$

The electromagnetic fields are given by the formulas of Appendix B, namely (B.9) to (B.14). The unkown constants R_m, Δ_m, F_m and G_m can be obtained by expressing the continuity of the tangential field components at $\rho = a$. This yields a system of four linear equations in these unkowns. With a view to future approximations we will however use an alternative but equivelent method.

Starting from (2.196) - (2.197), we express the fields in the external medium and, by eliminating the constants F_m and G_m, we can obtain two relations between

the tangential field components at $\rho = a$. These relations are written in the form

$$E_{\phi m} = \alpha_m E_{zm} + Z_m H_{zm} \quad (2.199)$$

$$H_{\phi m} = -Y_m E_{zm} + \alpha_m H_{zm} \quad (2.200)$$

for the m-th harmonic of the fields. After some calculations we find

$$\alpha_m = -\frac{jm\Gamma}{u^2 a} \quad (2.201)$$

$$Z_m = -\frac{j\omega\mu_1}{u} \frac{K_m'(ua)}{K_m(ua)} \quad (2.202)$$

$$Y_m = \frac{k_1^2}{j\omega\mu_1 u} \frac{K_m'(ua)}{K_m(ua)} \quad (2.203)$$

Equations (2.199) - (2.200) depend on the external medium only and, of course, on the still unknown propagation constant Γ. We could as well solve them for the electric field components $E_{\phi m}$ and E_{zm}, thereby defining a surface impedance matrix of the external medium. Equations (2.199) - (2.200) may thus be considered as boundary conditions imposed by the external medium and must be satisfied by the fields derived from (2.194) and (2.195) for the internal medium. Expressing this, we obtain after some calculations

$$R_m(\Gamma) = \frac{jk_o/v\, K_m'(va)/K_m(va) + \eta_o Y_m + \eta_o \delta_m}{jk_o/v\, I_m'(va)/I_m(va) + \eta_o Y_m + \eta_o \delta_m} \quad (2.204)$$

$$\Delta_m(\Gamma) = \left(\frac{K_m(va)}{I_m(va)} \frac{R_m - 1}{\eta_o}\right) \frac{\eta_o \delta_m}{(jm\Gamma/a)(v^{-2} - u^{-2})} \quad (2.205)$$

where $\eta_o = \sqrt{\mu_o/\varepsilon_o}$ is the intrinsic impedance of air and

$$\eta_o \delta_m = \frac{(jm\Gamma/a)^2 (v^{-2} - u^{-2})^2}{jk_o/v\, I_m'(va)/I_m(va) + Z_m/\eta_o} \quad (2.206)$$

Hence, the exact expressions are known for the potentials and fields inside the tunnel, but the propagation constant Γ is not yet determined. There indeed remains to express the boundary condition on the external surface of the cable. As we intend to use the thin-cable approximation, we first need to write explicitely the

expression of the axial field E_z. It is given by $(-v^2 U)$ as results from eq. (9.5) of Appendix B. Using (2.194) in which we restore the compact form (2.190) for the primary potential, we obtain

$$E_z = \frac{-v^2 I}{2\pi j\omega\mu_o}\left[K_o(v\rho_d) - \sum_{m=-\infty}^{\infty} R_m \frac{K_m(va)}{I_m(va)} I_m(v\rho_o)\, I_m(v\rho)\, e^{-jm(\phi-\phi_o)}\right] \qquad (2.207)$$

In this expression, the sum over m represents the field reflected by the tunnel wall and is assumed to be practically constant when the observation point moves around the cable circumference. This is the condition required for the thin-cable approximation to be valid. The boundary condition at the external surface of the cable may then be expressed at any point of this surface. Thus we choose the matching point at $\rho = \rho_o + c$ and $\phi = \phi_o$ and obtain the mode equation

$$K_o(vc) - \sum_{m=-\infty}^{\infty} R_m \frac{K_m(va)}{I_m(va)} I_m(v\rho_o)\, I_m[v(\rho_o + c)] = \frac{-2\pi j\omega\mu_o}{v^2} z_o(\Gamma) \qquad (2.208)$$

where $z_o(\Gamma)$ is the specific external impedance of the cable. This parameter is determined by the internal structure of the cable and may depend on the mode propagation constant Γ as we have seen in sections 2.5 and 2.5.6.

Solving the mode equation in full generality obviously requires the use of a computer. The method of Newton-Raphson for complex variables is claimed to be efficient for this purpose. The solution of the mode equation provides the propagation constant of all modes, including the waveguide modes. Of particular interest however are the modes which have a transmission-line character as the frequency is lowered or as the wall conductivity becomes very high. In case of a single monofilar wire conductor we will find one such mode, this is the monofilar mode. In case of a leaky coaxial cable we will find the monofilar and coaxial modes described in Chapter 1. Some interest nevertheless exists for the waveguide modes when they are above cutoff, since they may then have a lower specific attenuation than the transmission-line modes. It is expected that their cutoff frequencies will not be significantly modified by the presence of the cable.

It is unfortunately not possible to introduce approximations which are valid for all cases encountered in the practice of subsurface radio communications. If $|k_1 a| \gg 1$, we have also $|ua| \gg 1$ and asymptotic expressions of $K_m(ua)$, $K_m'(ua)$ may be used in the calculation of Y_m and Z_m, at least for moderate values of m.

However a look at Figure 1.2 shows that the condition $|k_1 a| \gg 1$ will not be satisfied for small tunnel radii, low wall conductivity and at low frequencies. When it is known that the mode propagation constant Γ is close to jk_o, i.e. for the monofilar mode, we have $|v| \ll k_o$ and Figure 1.2 shows that we may have $|va| \ll 1$ if the frequency is not too high. The conditions $|ua| \gg 1$ and $|va| \ll 1$ are obviously not frequently met simultaneously. The implications of these conditions will be examined later. Only the condition $|vc| \ll 1$ is satisfied over the whole range of parameters, but this brings very meagre simplification in the numerical work.

2.8.2. Extension to multiple wires or cables

It is now relatively easy to extend the theory to the case where the tunnel contains multiple wires or cables. We will carry out this extension to the case of two cables (Figure 2.11). The cables are located at the points (ρ_1, ϕ_1) and (ρ_2, ϕ_2). They have radii c_1, c_2 and specific external impedances $z_1(\Gamma)$, $z_2(\Gamma)$ respectively. The method (Wait and Hill, 1974b) consists of superposing solutions of the type (2.208). We write

$$E_z = \frac{-v^2}{2\pi j\omega\varepsilon_o}\left\{ I_1\left[K_o(v\rho_{d1}) - \sum_{m=-\infty}^{\infty} R_m \frac{K_m(va)}{I_m(va)} I_m(v\rho_1)\, I_m(v\rho)\, e^{-jm(\phi-\phi_1)}\right] + I_2\left[K_o(v\rho_{d2}) - \sum_{m=-\infty}^{\infty} R_m \frac{K_m(va)}{I_m(va)} I_m(v\rho_2)\, I_m(v\rho)\, e^{-jm(\phi-\phi_2)}\right]\right\} \qquad (2.209)$$

where

$$\rho_{d1} = \sqrt{\rho^2 + \rho_1^2 - 2\rho\rho_1 \cos(\phi - \phi_1)} \qquad (2.210)$$

$$\rho_{d2} = \sqrt{\rho^2 + \rho_2^2 - 2\rho\rho_2 \cos(\phi - \phi_2)} \qquad (2.211)$$

and I_1, I_2 are the currents carried by the cables.

The two relevant boundary conditions are now

$$E_z = z_1 I_1 \quad \text{at} \quad \rho = \rho_1 + c_1\,,\ \phi = \phi_1 \qquad (2.212)$$

$$E_z = z_2 I_2 \quad \text{at} \quad \rho = \rho_2 + c_2\,,\ \phi = \phi_2 \qquad (2.213)$$

This yields a homogeneous system of two equations into I_1, I_2

$$A_{11} I_1 + A_{12} I_2 = 0 \qquad (2.214)$$

$$A_{21} I_1 + A_{22} I_2 = 0 \qquad (2.215)$$

with

$$A_{11} = \frac{2\pi j k_o z_1}{v^2 \eta_o} + K_o(vc_1) - \sum_m R_m \frac{K_m(va)}{I_m(va)} I_m(v\rho_1) I_m\left[v(\rho_1 + c_1)\right] \qquad (2.218)$$

$$A_{12} = K_o(v\rho_{12}) - \sum_m R_m \frac{K_m(va)}{I_m(va)} I_m(v\rho_2) I_m\left[v(\rho_1 + c_1)\right] e^{-jm(\phi_1 - \phi_2)} \qquad (2.217)$$

$$A_{21} = K_o(v\rho_{12}) - \sum_m R_m \frac{K_m(va)}{I_m(va)} I_m(v\rho_1) I_m\left[v(\rho_2 + c_2)\right] e^{-jm(\phi_2 - \phi_1)} \qquad (2.216)$$

$$A_{22} = \frac{2\pi j k_o z_2}{v^2 \eta_o} + K_o(vc_2) - \sum_m R_m \frac{K_m(va)}{I_m(va)} I_m(v\rho_2) I_m\left[v(\rho_2 + c_2)\right] \qquad (2.219)$$

Actually, the argument of K_o in (2.217) should be $v\rho_{d2}$ evaluated at the matching point $\rho = \rho_1 + c_1$, $\phi = \phi_1$ but ρ_{d1} has been approximated by the distance between the cable centers :

$$\rho_{12} = \sqrt{\rho_1^2 + \rho_2^2 - 2\rho_1\rho_2 \cos(\phi_1 - \phi_2)}. \qquad (2.220)$$

It must indeed be stressed that the use of the thin-cable approximation in this problem requires the cable radii c_1, c_2 to be small compared to ρ_{12}. The same approximation has been made in A_{21}.

The mode equation is obtained by writing that the determinant of the system (2.214) - (2.215) is zero. Once it has been solved, the ratio I_2/I_1 is given by any one of the equations (2.214) - (2.215). This ratio thus takes a well-defined value for each guided mode. For instance, in the case of a bifiler line or of the long induction loop, there are two modes having a transmission-line character. These modes, which are designated the monofiler and bifilar modes, have I_2/I_1 ratios close to + 1 and - 1, respectively.

2.8.3. Discussion of some numerical results

The theory contained in the previous two sections has been applied, mainly by Wait, Hill and Seidel to numerous examples. For the case of one or two isolated wires strung into a tunnel, remarkable qualitative and quantitative confirmations of results given in Chapter 1 are obtained.

Results have also been obtained for leaky coaxial cables. The model used for calculating the specific external impedance of a leaky coaxial cable was developed in section 2.5.2. This impedance is strongly dependent on the longitudinal propagation constant Γ and is reactive if the cable is lossless.

As a useful exercise, before showing results obtained for the case of tunnels we will investigate the behaviour of a leaky coaxial cable drawn into free space. For greater simplicity, we will assume that the inner conductor has an infinite conductivity and that the shield is uncoated. The specific external impedance of the cable is then given by (2.77) which will be rewritten as

$$z_o = j\omega m_t \frac{\beta^2 - \beta_{co}^2}{\beta^2 - \beta_\infty^2} \qquad (2.221)$$

where $\beta_{co} = k_o \sqrt{\kappa}$ is the phase constant of a perfectly shielded cable, κ being the dielectric constant of the cable insulation and

$$\beta_\infty = \beta_{co} \sqrt{1 + m_t/l_o} \qquad (2.222)$$

In the external air medium, the transverse fields are given by

$$E_{zo} = - v^2 K_o(v\rho) \qquad (2.223)$$

$$H_{\phi o} = -j\omega\varepsilon_o v K_o'(v\rho) \qquad (2.224)$$

Using small-argument approximations for the modified Bessel function and writing that $z_o = E_{zo}/(2\pi c H_{\phi o})$, where c is the cable radius, we obtain

$$- \ln \frac{C c \sqrt{\beta^2 - k_o^2}}{2} = \frac{2\pi k_o \omega m_t}{\eta_o} \frac{\beta^2 - \beta_{co}^2}{(\beta^2 - k_o^2)(\beta^2 - \beta_\infty^2)} \qquad (2.225)$$

The right-hand side of this equation is shown on Figure 2.12 as a function of

β/k_o for a particular choice of parameters. The left-hand side is real for $\beta > k_o$ only. It is a relatively large positive quantity (larger than 5 on Figure 2.12) and a slowly varying function of β. Consequently, eq. (2.225) has two roots β_m and β_c which are slightly higher than k_o and $\beta_=$, respectively. They correspond to the monofilar and coaxial modes of the structure in free space. Both waves are slow compared with the velocity of light in free space and, consequently, they have a surface wave character. It is remarkable that the coaxial mode is even slower than that of a perfectly shielded cable; this is due to the reactive loading of the leaky shield. Actually the term leaky is misleading since it is generally used for fast wave structures (Collin and Zucker, 1969). It has some importance to keep these properties in mind, and namely Table 1.2, when we try to interprete physically the behaviour of leaky coaxial cables used in tunnels.

Some results of calculations for a leaky coaxial cable drawn longitudinally inside a tunnel were published (Wait and Hill, 1975b, 1976c; Hill and Wait, 1978b). As it does not much complicate the numerical work, it has been assumed that the cable shield is covered by a dielectric jacket. The latter may be covered itself by a lossy film which may represent moisture and dust accumulated on the cable. Figure 2.13 exhibits the specific attenuation of the monofilar mode for the conditions specified in the legend.

We have selected the curves of Figure 2.14 a and b for the attenuation of the coaxial mode. For a cable with a very high specific transfer inductance (m_t = 40 nH/m) the attenuation is very sensitive to close proximity of the wall. For a moderate transfer inductance (10 nH/m) this effect is rather limited. It is unnoticeable for well-shielded cables (2 nH/m). In any case, the attenuation is undistinguishable from its free-space value when the cable lies along the tunnel axis. It is then essentially due to the finite resistivity of the inner conductor, since the resistance of the shield was neglected in the calculations. We have some doubts on the quantitative values of attenuation for ρ_o/a = 0.98 since the thin-cable approximation is somewhat questionable in these conditions. The result is however qualitatively satisfactory.

2.8.4. Quasi-static approach

The exact theory of wave propagation along wires and cables strung in a circular tunnel as developed in sections 2.8.1 and 2.8.2 is extremely complex. It would be nice to obtain a simpler description, not only to justify heuristic approaches like those given in Chapter 1, but also to support extensions to other tunnel shapes for which a theoretical approach is untractable.

The quite tedious task of making approximations in the complicated equations of sections 2.8.1 and 2.8.2 was undertaken. We will summarize briefly the fundamental conclusions of this study. Let us recall that, for a mode with a propagation constant Γ, we defined two transverse propagation constants. The first one

$$v = (- k_o^2 - \Gamma^2)^{1/2} \tag{2.226}$$

is valid for the tunnel space, whereas the other one

$$u = (- k_1^2 - \Gamma^2)^{1/2} \tag{2.227}$$

is valid for the tunnel wall material. The wave numbers k_o and k_1, respectively in the air and in the wall material are related through

$$k_1^2 = k_o^2 \kappa_1'$$

$$= k_o \left[\kappa_1 - j \frac{\sigma_1}{\omega \epsilon_o}\right] \tag{2.228}$$

where κ_1 and σ_1 are the wall permittivity and conductivity, respectively. We also use the notation $\gamma_1 = jk_1$.

Three parameters govern the possibility of making approximations

1. va : as generally Γ does not differ significantly from k_o, the condition $|va| << 1$ is generally satisfied when the tunnel cross-section is smaller than the free-space wavelength. this practically occurs at frequencies up to 50 to 100 MHz.

2. $|\kappa_1'| >> 1$: this occurs at low frequencies because of the tunnel wall conductivity, and at higher frequencies if the dielectric constant κ_1 is high. this will namely occur if the tunnel walls are humid.

3. $|\gamma_1 a|$: this parameter describes the ratio of the tunnel radius to the penetration depth of electromagnetic waves into the tunnel material. At low frequencies the skin depth is much larger than the tunnel radius and we have $|\gamma_1 a| << 1$. At high frequencies the reverse occurs.

The conclusions are as follows. Provided $|va| << 1$ and $|\kappa_1'| >> 1$, which is true over a very large frequency range, the transverse electric field in the tunnel space is roughly the same as for the TEM mode with a perfectly conducting tunnel wall, even if the skin depth into the actual wall is larger than the tunnel size. This entails that we may write transmission lines of the form

$$-\frac{dI}{dz} = j\omega c\, V \qquad (2.229)$$

when the currents and voltages are those of the conductors, and the specific capacity coefficients may be evaluated under the assumption of a perfectly conducting tunnel wall.

Under the same conditions, the transverse magnetic field in the tunnel space does not depend on the mode propagation constant Γ. Therefore it will have the same spatial distribution, for instance, for the coaxial and monofilar modes of a leaky feeder. This distribution is however frequency dependent, being governed by the parameter $\gamma_1 a$. At low frequencies, for which $|\gamma_1 a| << 1$, the current in the tunnel wall is spread in a very large area and the magnetic field in the tunnel space can be calculated from the cables currents by Biot-Savart law, ignoring the tunnel wall current. At high frequencies, for which $|\gamma_1 a| >> 1$, the current in the tunnel wall is close to the surface and the magnetic field distribution tends to be the same as for a perfectly conducting tunnel wall.

It is possible to write a second transmission line equation of the type

$$-\frac{dV}{dz} = z\, I$$

but the evaluation of z may require more sophisticated methods.

2.9. OTHER PROBLEMS

Many other problems pertaining to electromagnetic theory are of interest for subsurface radio propagation. Some of them are solved in the author's book mentioned in section 1.1 and to which the interested reader is referred for further study.

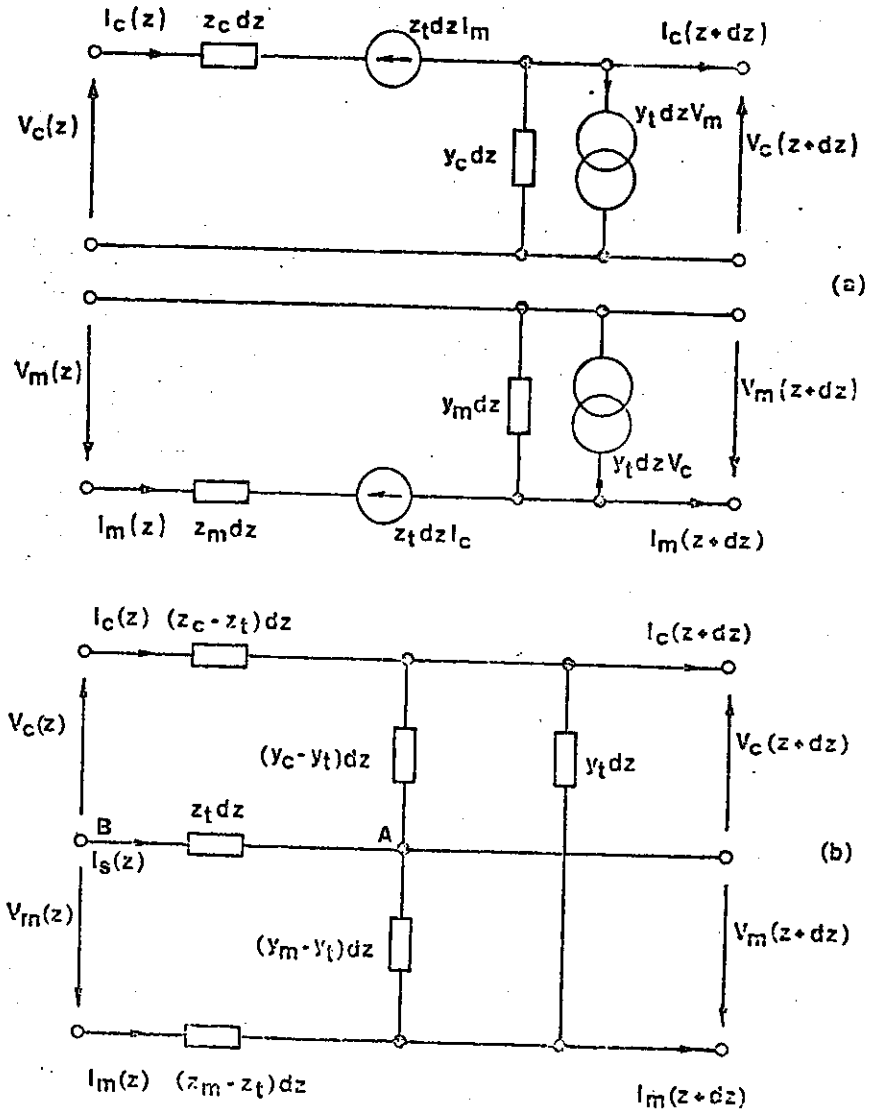

Fig. 2.1 Two equivalent circuits of an elementary length dz of two coupled transmission lines.

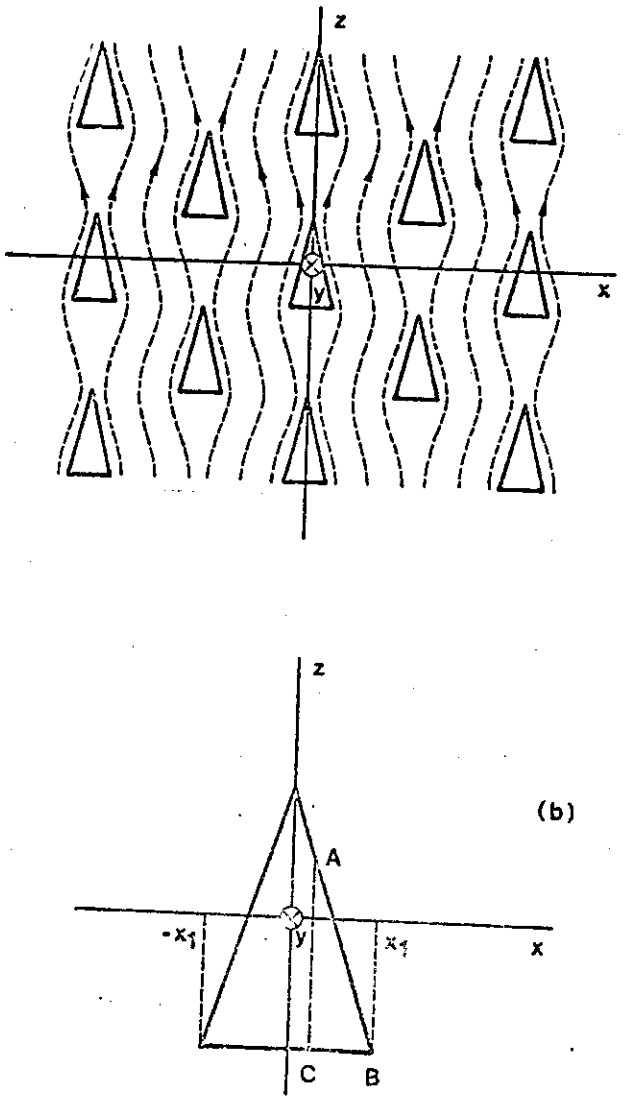

Fig. 2.2 Plane shield with a periodic distribution of apertures.

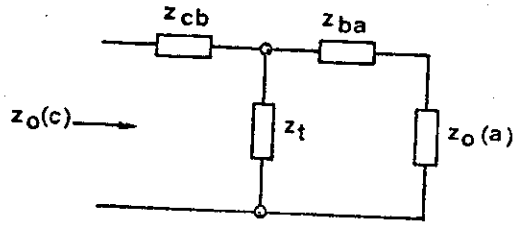

Fig. 2.3 The equivalent ladder network for the external specific impedance of a leaky cable with external coating.

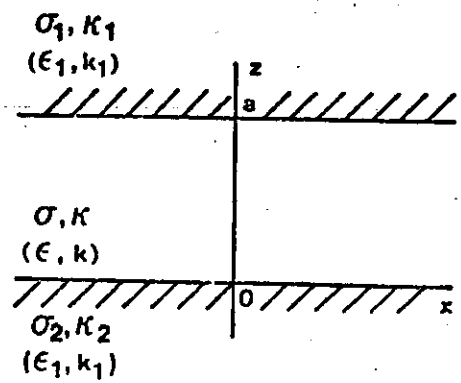

Fig. 2.4 Low-conductivity layer embedded between two semi-infinite half-spaces of higher conductivity.

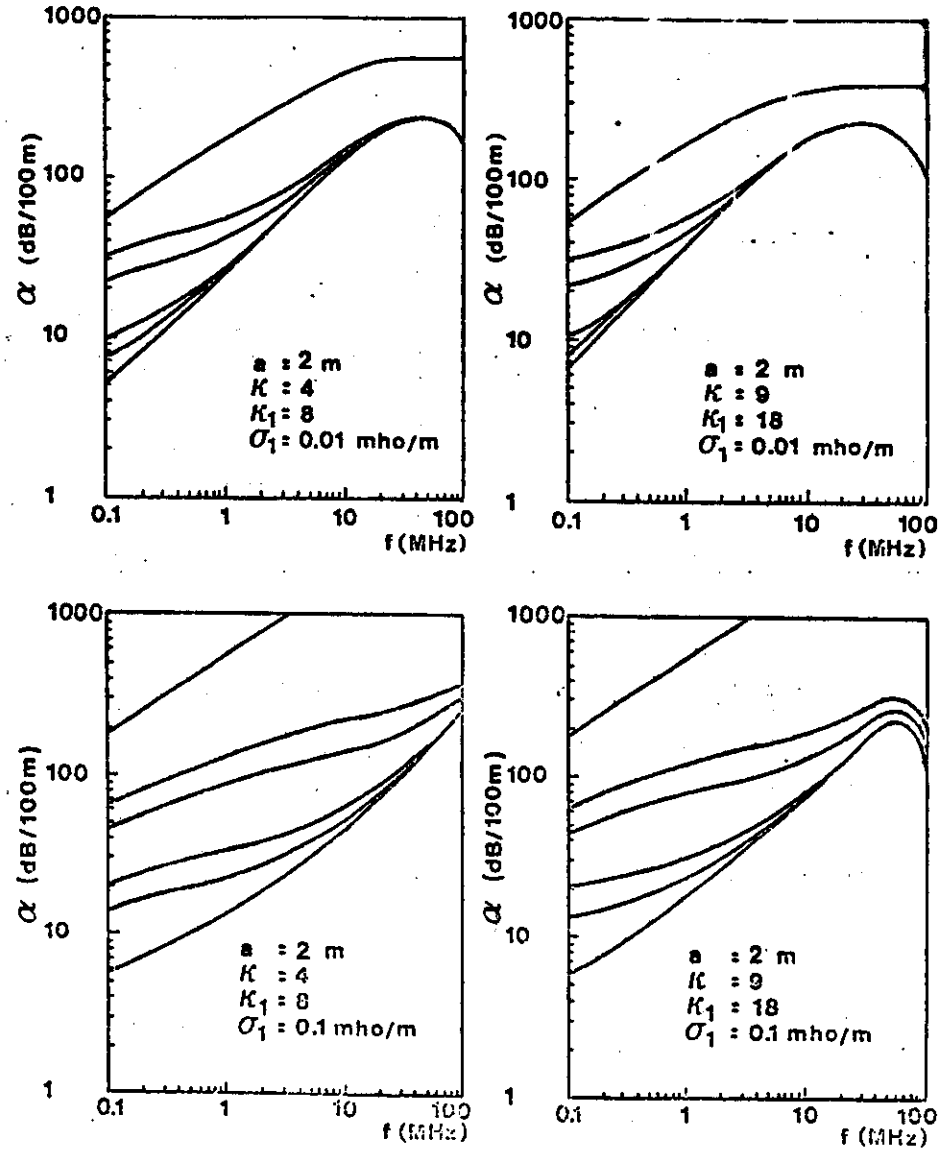

Fig. 2.5.a Specific attenuation of the dominant mode in a coal seam with thickness 2 meter.

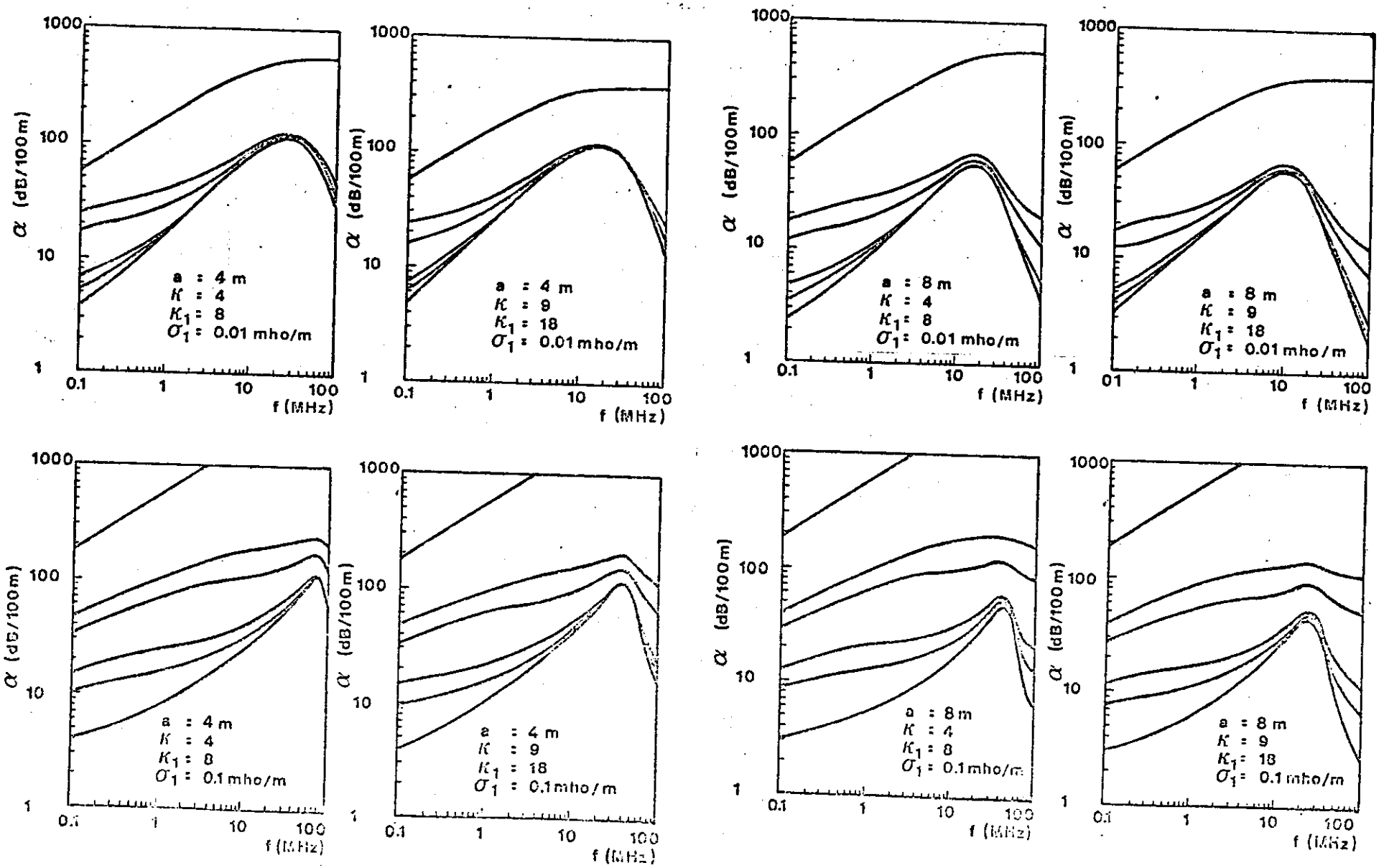

Fig. 2.5.b Specific attenuation of the dominant mode in a coal seam with thickness 4 meter.

Fig. 2.5.c Specific attenuation of the dominant mode in a coal seam with thickness 8 meter.

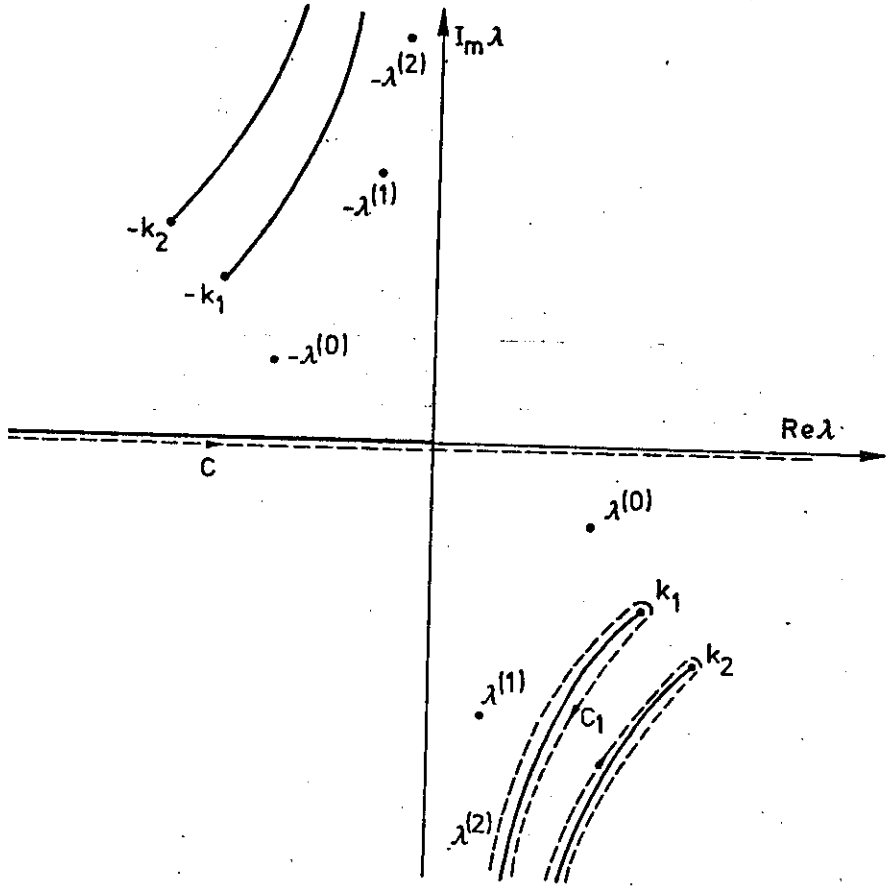

Fig. 2.6 Singularities of the integrand of (2.107) in the complex λ-plane

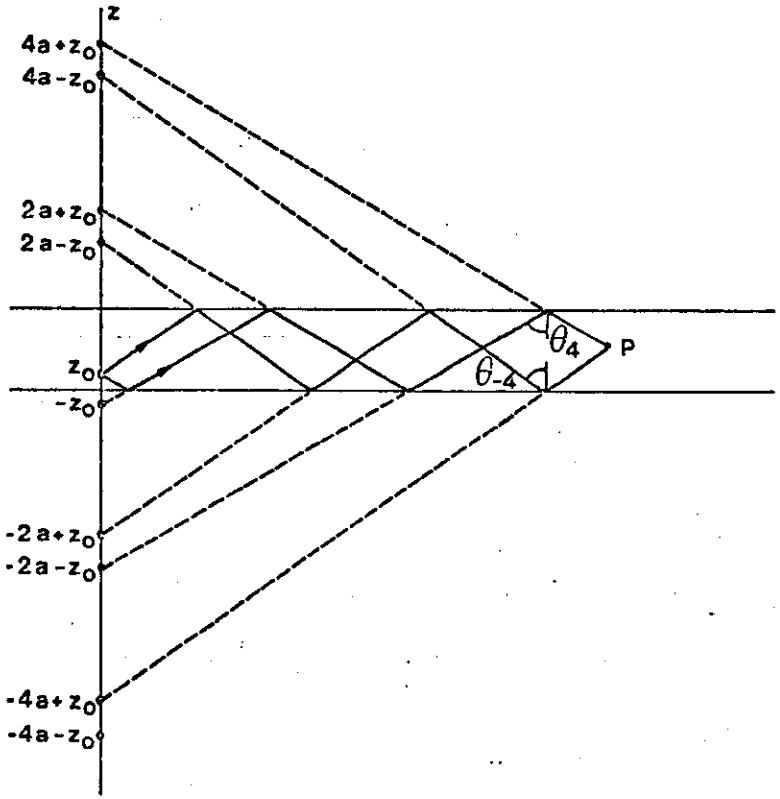

Fig. 2.7 Geometrical optical approach. The drawing shows the double infinity of images and the two rays undergoing four reflections.

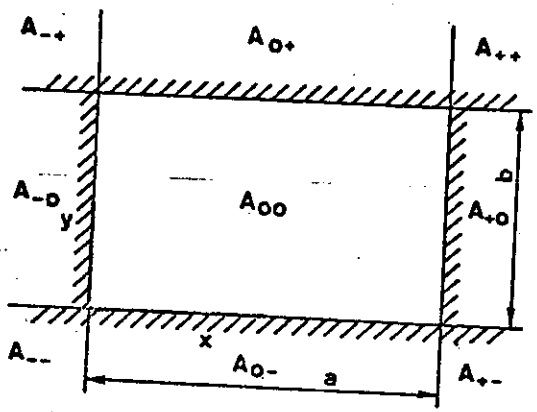

Fig. 2.8 Geometrical parameters for the rectenguler tunnel.

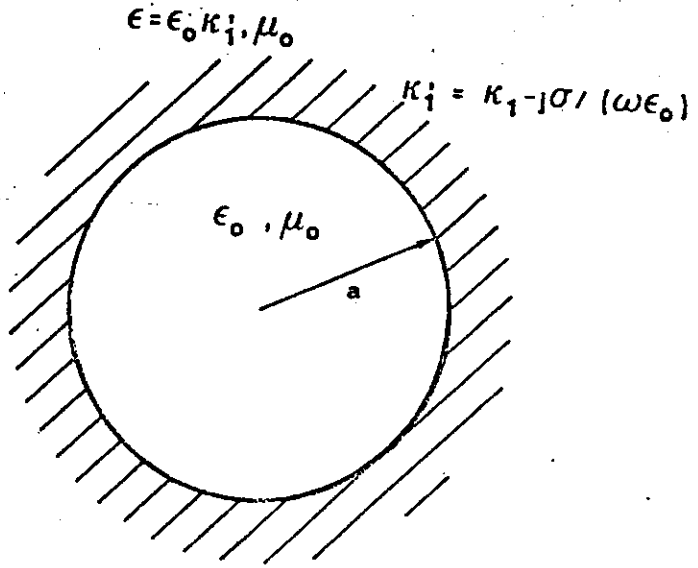

Fig. 2.9 Geometrical and electrical parameters of a circular tunnel.

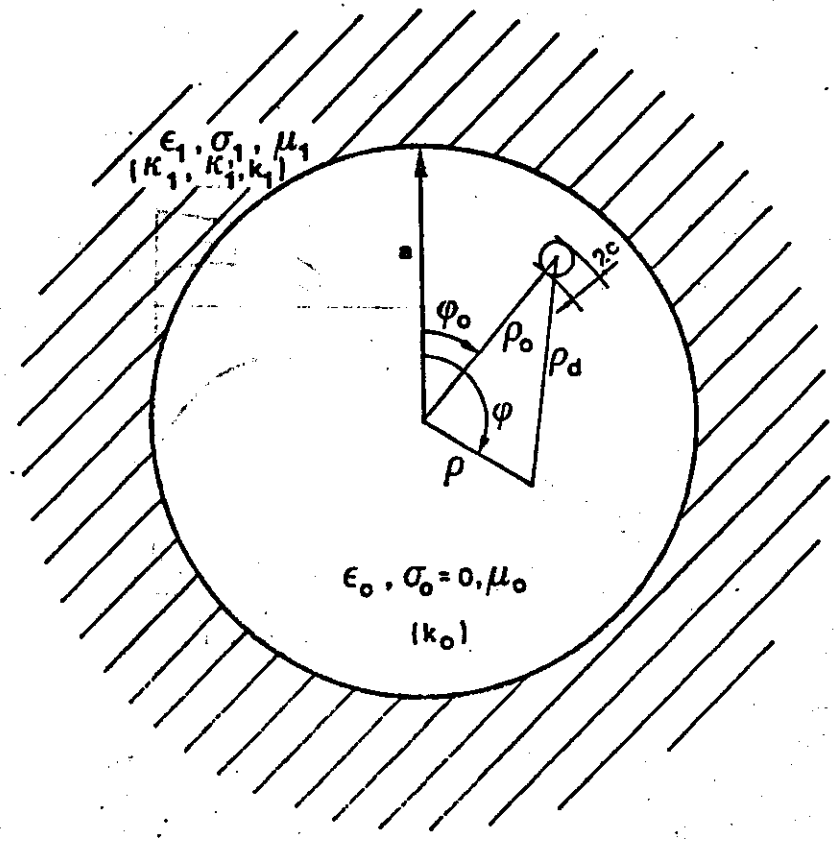

Fig. 2.10 Geometrical and electrical parameters for a single cable in a circular tunnel.

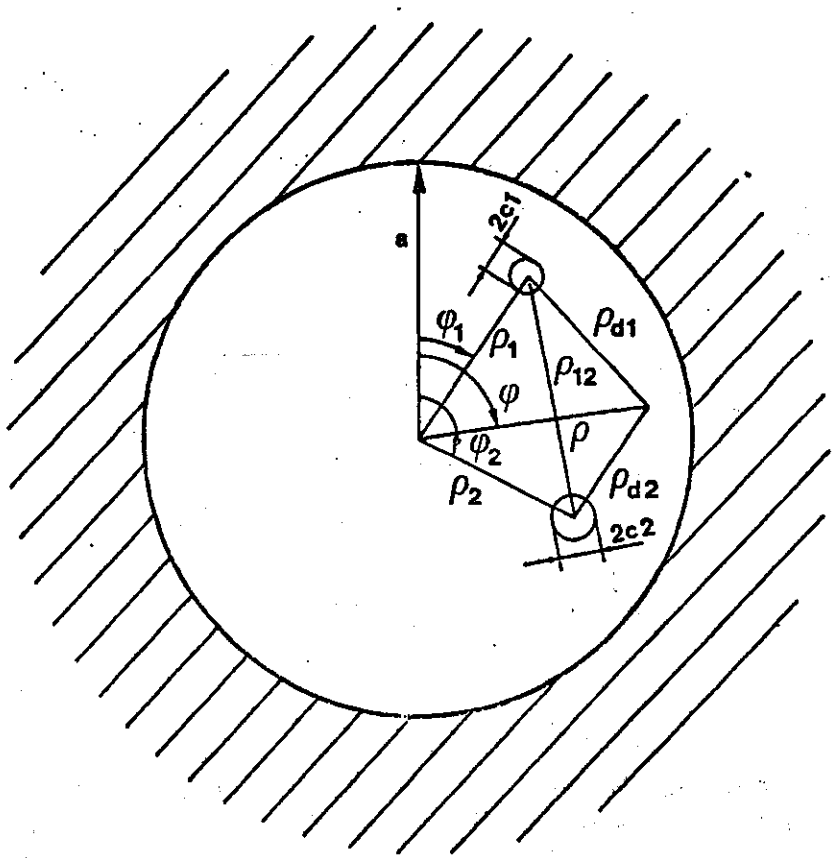

Fig. 2.11 Geometrical parameters for a circular tunnel containing two longitudinal cables.

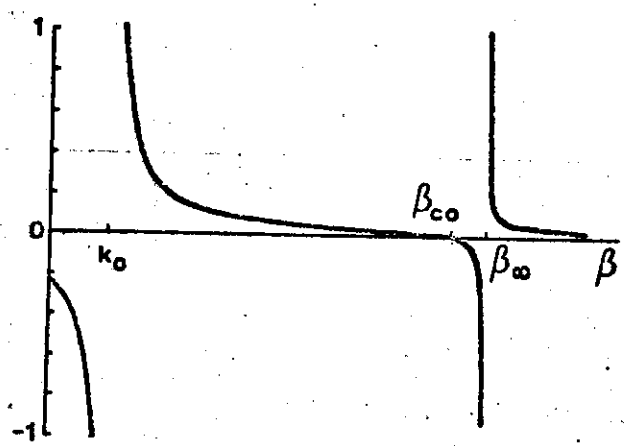

Fig. 2.12 The right-hand side of (2.376) as a function of β. Calculations have been made for f = 30 MHz, c = 5 mm, $\kappa = 2.5$, l_0 = 263.5 nH/m (50 ohm cable) and m_t = 20 nH/m.

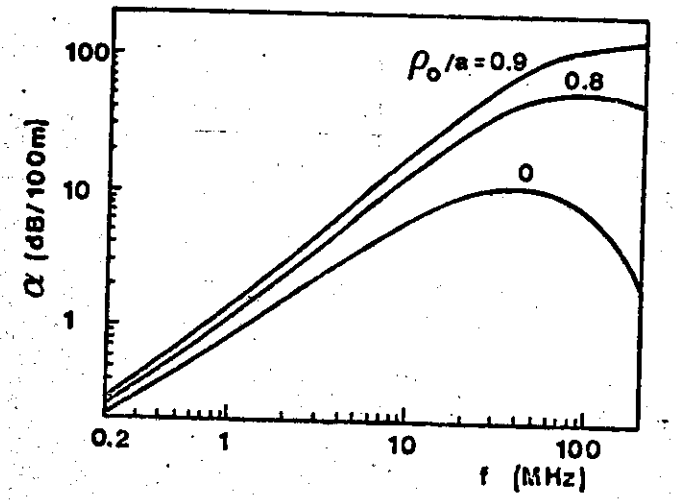

Fig. 2.13 Specific attenuation of the monofilar mode of a leaky coaxial cable for a = 2 m, κ_1 = 10, $\sigma_1 = 10^{-2}$ mho/m. Inner conductor : radius 1.5 mm, $\sigma = 5.7\ 10^7$ mho/m. Shield : radius 10 mm, m_t = 40 nH/m. Plastic jacket : radius 11.5 mm, $\kappa_j = 3$. No lossy film.

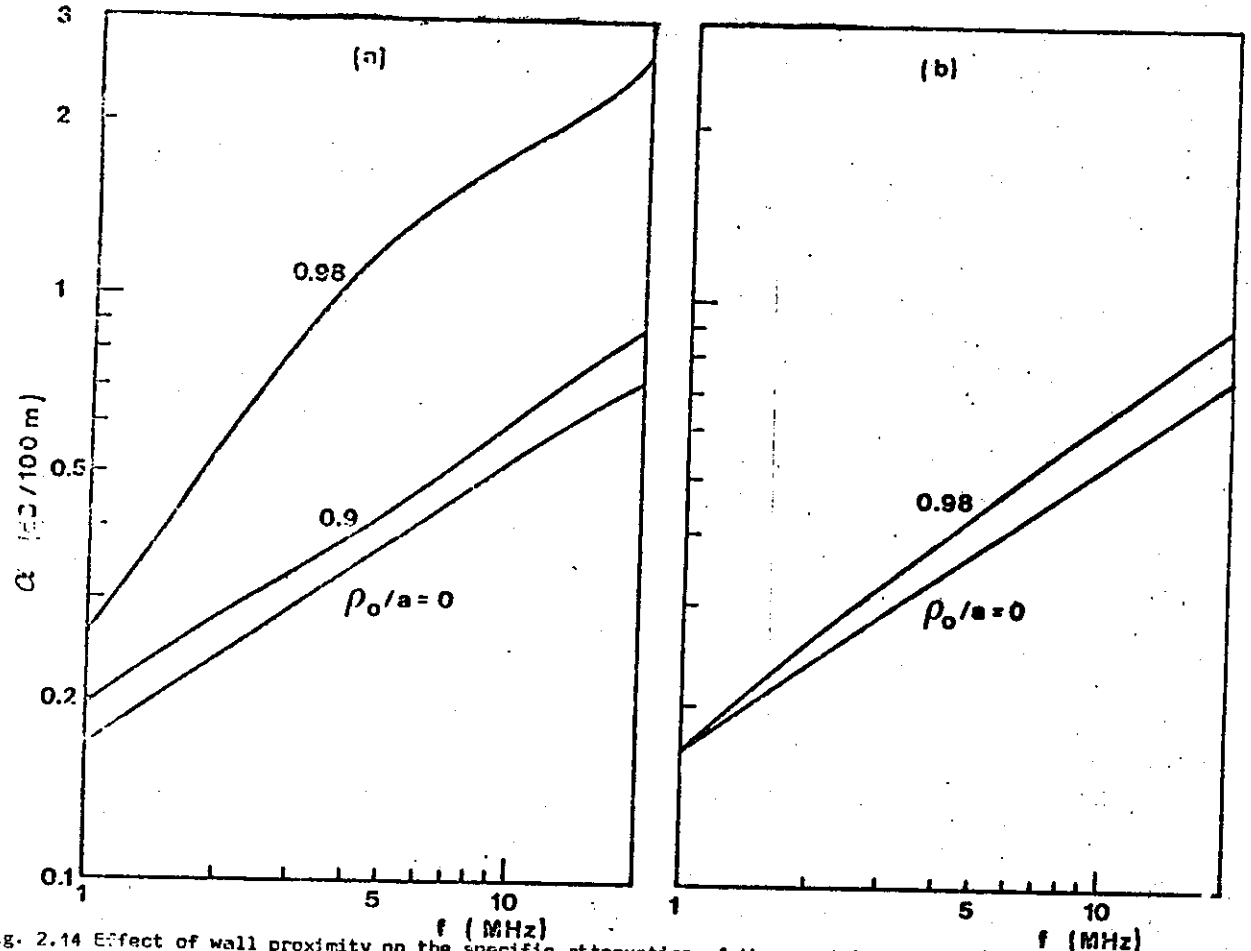

Fig. 2.14 Effect of wall proximity on the specific attenuation of the coaxial mode for a leaky feeder : (a) for m_t = 40 nH/m (b) for m_t = 10 nH/m. The other parameters are a=2 m, σ_g= 10^{-3} mho/m, κ_1=10. Internal conductor : copper, 1.5 mm radius. Insulation : κ=2.5 Outer conductor radius 10 mm. Jacket thickness 1.5 mm and dielectric constant 3.